AGU PUBLICATIONS

Tectonics

RESEARCH ARTICLE
10.1002/2014TC003768

Key Points:
- U-Pb zircon ages from North Makran granitoids track Eurasia evolution
- Sr-Nd isotopes show increasing mantle component with younging
- North Makran was an extensional system in Jurassic times

Supporting Information:
- Text S1
- Text S2
- Text S3
- Table S1
- Table S2
- Table S3
- Table S4

Correspondence to:
D. Hunziker,
daniela.hunziker@erdw.ethz.ch

Citation:
Hunziker, D., J.-P. Burg, P. Bouilhol, and A. von Quadt (2015), Jurassic rifting at the Eurasian Tethys margin: Geochemical and geochronological constraints from granitoids of North Makran, southeastern Iran, *Tectonics*, *34*, 571–593, doi:10.1002/2014TC003768.

Received 27 OCT 2014
Accepted 19 FEB 2015
Accepted article online 22 FEB 2015
Published online 24 MAR 2015

Jurassic rifting at the Eurasian Tethys margin: Geochemical and geochronological constraints from granitoids of North Makran, southeastern Iran

Daniela Hunziker[1], Jean-Pierre Burg[1], Pierre Bouilhol[2], and Albrecht von Quadt[1]

[1]Department of Earth Sciences, ETH Zurich, Zurich, Switzerland, [2]Durham University, Durham, UK

Abstract This study focuses on an east-west trending belt of granitic to intermediate intrusions and their volcanic cover in the northern Dur Kan Complex, a continental slice outcropping to the north of the exposed Makran accretionary wedge in southeastern Iran. Field observations, petrographic descriptions, trace element, and isotope analyses combined with U-Pb zircon geochronology are presented to determine the time frame of magmatism and tectonic setting during the formation of these rocks. Results document three magmatic episodes with different melt sources for (1) granites, (2) a diorite-trondhjemite-plagiogranite sequence, and (3) diabases and lavas. Granites, dated at 170–175 Ma, represent crystallized melt with a strong continental isotopic contribution. The diorite-trondhjemite-plagiogranite sequence is 165–153 Ma old and derives from a mantle magma source with minor continental contribution. East-west trending diabase dikes and bodies intruded the granitoids, which were eroded and then covered by Valanginian (140–133 Ma) alkaline lavas and sediments. Alkaline dikes and lavas have a mantle isotopic composition. Temporal correlation with plutonites of the Sanandaj-Sirjan Zone to the northwest defines a narrow, NW-SE striking and nearly 2000 km long belt of Jurassic intrusions. The increasing mantle influence in the magma sources is explained by thinning of continental lithosphere and related mantle upwelling/decompression melting. Accordingly, the formation of the studied igneous rocks is related to the extension of the Iranian continental margin, which ultimately led to the formation of the Tethys-related North Makran Ophiolites.

1. Introduction

Remnants of the Tethys Ocean in North Makran (Figure 1) are part of the southeastern Iranian segment of the Alpine-Himalayan orogeny [e.g., *Şengör*, 1990; *McCall*, 1997]. The temporal concept of the magmatic and geodynamic evolution of North Makran has been the subject of few works [e.g., *McCall*, 1997] compared to the sedimentary and tectonic evolution of the inland Makran accretionary wedge [*Carter et al.*, 2010; *Haghipour et al.*, 2012; *Burg et al.*, 2013; *Ruh et al.*, 2013]. Hence, most age constraints are based on microfossils, which dominantly yielded Early to Late Cretaceous ages [*Arshadi-Khamseh*, 1982; *McCall et al.*, 1985; *Dolati*, 2010]. A sequence of intermediate to felsic intrusions, unconformably covered by basaltic to trachyandesitic lava and pelagic sediments, has been interpreted as the most differentiated lithology of the North Makran Ophiolites [*Berberian and King*, 1981; *McCall and Kidd*, 1982; *McCall*, 2002; *Shahabpour*, 2010]. These rocks, however, show similarities to granite intrusions described in a narrow sliver of continental crust, the Dur Kan Complex (Figure 2) and its northwestward continuation, the Sanandaj-Sirjan Zone (Figure 1) [*McCall et al.*, 1985].

Intermediate to felsic rocks in the Sanandaj-Sirjan Zone have been ascribed to a magmatic arc produced on the Eurasian continent above the subduction of the Tethys oceanic lithosphere [e.g., *Berberian and King*, 1981; *Agard et al.*, 2005; *Khalaji et al.*, 2007; *Mazhari et al.*, 2009]. Some authors [e.g., *Stampfli and Borel*, 2002; *Ahmadi-Khalaji et al.*, 2007; *Shahbazi et al.*, 2010; *Ahadnejad et al.*, 2011; *Esna-Ashari et al.*, 2012] ascribed the calc-alkaline to tholeiitic Sanandaj-Sirjan Zone granitoids with Jurassic ages (187–144 Ma) as evidence for an already active subduction, although plate tectonic reconstructions based on paleomagnetic data ascertain that the Tethys Ocean was still opening, Pangea was still breaking up, and the Paleotethys, to the north, was still closing at that time [e.g., *Savostin et al.*, 1986; *Westphal et al.*, 1986; *Ricou*, 1994; *Scotese*, 2004]. Magmatic activity actually increased in the Late Cretaceous (<80 Ma), but it is associated to both the Sanandaj-Sirjan Zone and the Urumieh-Dokhtar magmatic arc (Figure 1) [e.g., *Farhoudi and Karig*, 1977; *Berberian and King*, 1981; *Alavi*, 1996; *Omrani et al.*, 2008]. Most authors agree that subduction in the Makran area was initiated

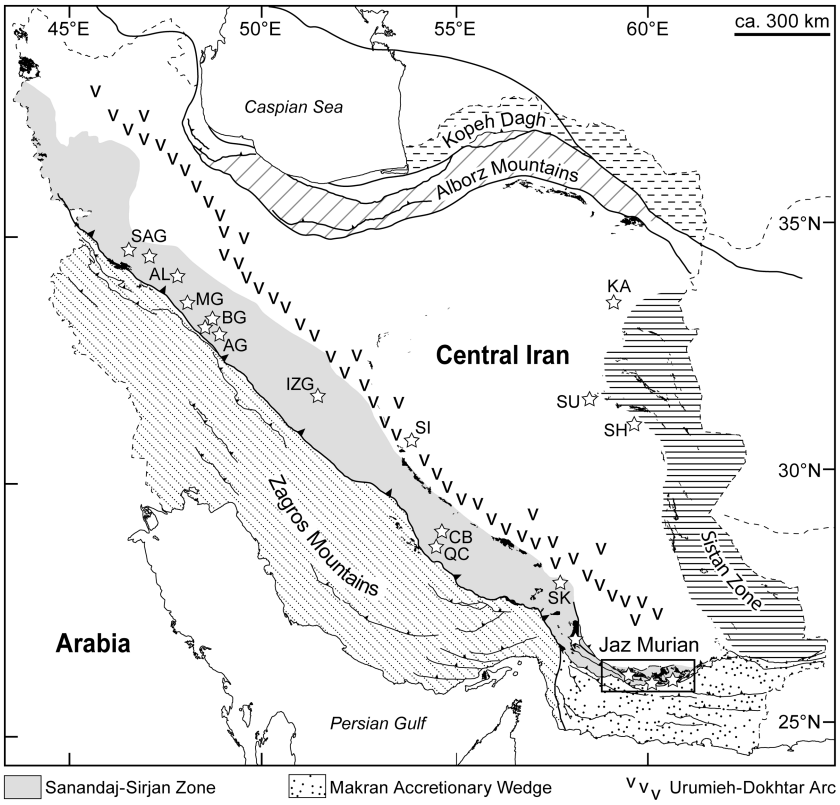

Figure 1. Tectonic units of Iran with Tethys-related ophiolite complexes (black) and Jurassic granitoids (stars). Aligoodarz granitoids after *Esna-Ashari et al.* [2012]; Alvand plutonic complex after *Shahbazi et al.* [2010]; Boroujerd granitoids after *Ahmadi-Khalaji et al.* [2007]; Inner Zagros granitoids after *Omrani et al.* [2008]; Malayer granitoids after *Aghazadeh et al.* [2010]; Suffi Abad granitoids after *Azizi et al.* [2011]; Klateh Ahari, Shah Kuh, and Surkh Kuh granitoids after *Karimpour et al.* [2011]; Qori Complex after *Fazlnia et al.* [2009]; and Shir Kuh from *Esmaeily et al.* [2005]. Rectangle = study area, Figure 2. The spelling of Persian names is taken from published reports of the Geological Survey of Iran.

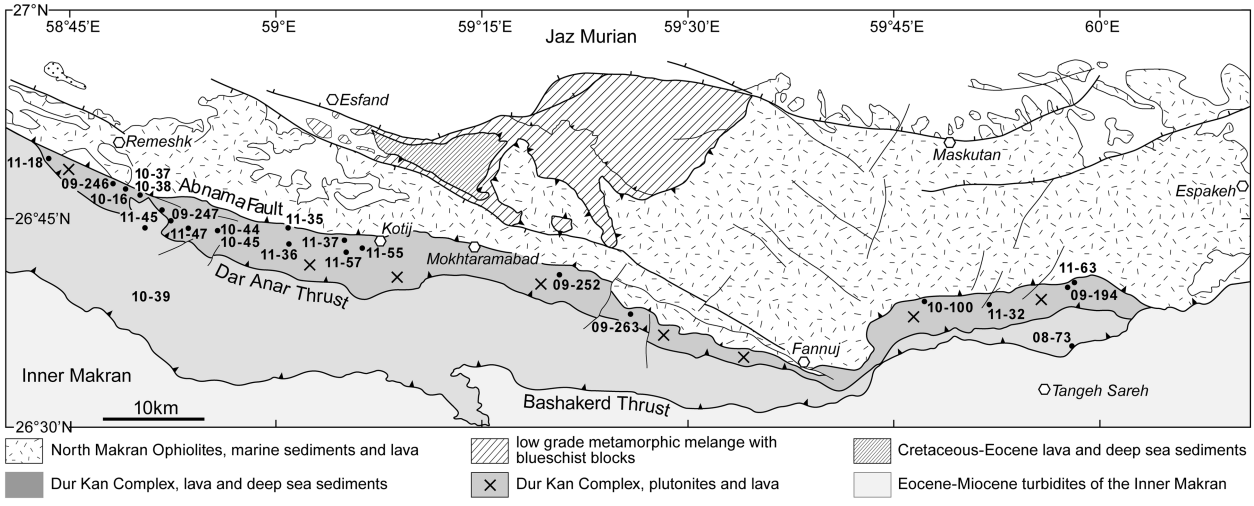

Figure 2. Simplified geological map of North Makran with their location (numbered dots) of samples used for geochemical analyses (see also Table 1). Hexagons = townships. Location in Figure 1. Coordinates and outcrop descriptions in Appendix Table S2 in the supporting information..

only in Late Cretaceous times [*Berberian and King*, 1981; *Desmons and Beccaluva*, 1983; *Babaie et al.*, 2001]. This study of North Makran granitoids reopens the discussion on whether subduction in Makran was initiated earlier than assumed or if Jurassic magmatism along the southern Eurasian margin developed in a different geotectonic setting. The ~80 Ma age gap between the reportedly subduction-related Jurassic granitoids in the Sanandaj-Sirjan Zone and the earliest reported Late Cretaceous magmatism in the Urumieh-Dokhtar volcanic arc questions the geotectonic affinity of the Sanandaj-Sirjan Zone and North Makran within the frame of the Tethys history.

This study was carried out to specify the origin of the North Makran intermediate to felsic rocks and identify the geodynamic affiliation and temporal relation with neighboring Tethyan suture zones. Field and geochemical investigations indicate a strong continental contribution in the oldest granite magma source and an increasingly mantle-derived source for the younger granitoids. In contrast, the overlying alkaline volcanic rocks have a strong mantle affinity and do not show any significant crustal contribution. Petrological and geochemical characterizations of the granitoids point to calc-alkaline and alkaline to low-K tholeiitic magmatism into a continental crust. The increasing mantle influence in the magma source is explained by thinning of the continental lithosphere and related mantle upwelling. This extensional event may have led to the formation of the North Makran Ophiolites (Figure 2) in a hitherto unrecognized marginal basin.

2. Geological Setting

2.1. North Makran

The Makran region exposes the east-west trending emerged portion of the accretionary wedge built above the still active north dipping subduction, whose current trench is in the Oman Sea farther south [e.g., *McCall and Kidd*, 1982; *Dercourt et al.*, 1986; *Bayer et al.*, 2006; *Vigny et al.*, 2006; *Burg et al.*, 2013]. North Makran is bordered by the Jaz Murian depression to the north. To the south, the Bashakerd Thrust places North Makran over the Eocene turbidites and lavas of Inner Makran (Figure 2) [*Dolati*, 2010; *Burg et al.*, 2013]. North Makran exposes ophiolites, "colored mélanges," Cretaceous volcanic units, and Cretaceous to present-day sedimentary sequences [e.g., *Eftekhar-Nezhad et al.*, 1979; *McCall et al.*, 1985; *McCall*, 2002]. The ophiolites were interpreted as pieces of Tethys oceanic lithosphere now accreted to the Gondwana-derived Central Iran microcontinent (Figure 1) [*McCall et al.*, 1985; *Ricou*, 1994; *Şengör*, 1990]. They are unconformably covered by Late Cretaceous lavas, volcanoclastic turbidites, and shallow water limestone.

At variance with previous studies [e.g., *McCall et al.*, 1985; *McCall*, 2002], we assigned the intermediate to felsic rocks to the Dur Kan Complex rather than to the North Makran Ophiolites, because the Abnama Fault (Figure 2) separates these granitoids from the ophiolitic rocks, and no primary contact was found. The north dipping Abnama thrust fault carried the North Makran Ophiolites southwestward (Figure 3) on the Dur Kan Complex, which is an assemblage of plutonic bodies covered by Cretaceous lava and shallow and deep marine Permian to Cretaceous sediments (Figure 2) [*McCall et al.*, 1985]. The Dur Kan Complex has been interpreted as an ~250 km long and $<$40 km wide slice of continental crust that separates the ophiolites from the turbiditic to neritic sediments accumulated in a mobile trench to the south [*Berberian and King*, 1981; *McCall and Kidd*, 1982; *McCall*, 1997]. Satellite images and field observations were used to define the Dur Kan Complex as the southeastern continuation of the Sanandaj-Sirjan Zone [*Berberian and King*, 1981; *McCall and Kidd*, 1982; *McCall et al.*, 1985; *Şengör*, 1990; *McCall*, 1997; *Dilek et al.*, 1999; *McCall*, 2002; *Agard et al.*, 2005].

2.2. Study Area

The study area covers an ~200 km long and up to 20 km wide band of the nearly east-west trending northern Dur Kan Complex (Figure 2), where most granitoids occur. The WNW-ESE striking Dar Anar Thrust separates the northern from the southern Dur Kan Complex down to Fannuj Township, where a marked structural bend links the eastern and western domains (Figure 2). To the east of Fannuj, trondhjemites form a several hundred meters long and wide body, which is unconformably covered by lava (Figure 4a) so that trondhjemite is also found in valleys incised deep enough to reach below the base of lava flows. Other trondhjemite outcrops are mostly fragmented and constitute enclaves of several meters to tens of meter size in lavas (Figure 4b).

Most of the intermediate to felsic plutonic rocks are located to the west of Fannuj, to the south of the Abnama Fault between Remeshk and Kotij (Figure 2), where trondhjemite, diorite, plagiogranite, and granite bodies (greater than tens of square kilometers) are intruded by east-west striking diabase dikes.

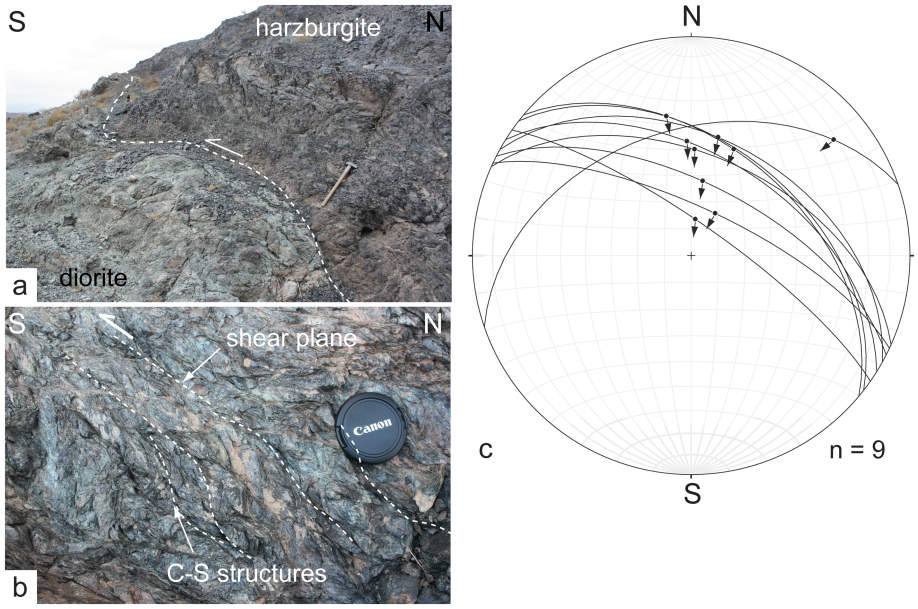

Figure 3. Contact of the Dur Kan Complex with the North Makran Ophiolites. (a) Harzburgite thrust on diorite (N026°44′23.8″/E059°01′12.5″). (b) Asymmetric lens-shaped structures (dashed lines) defining top to SSW thrusting in harzburgite (N026°38′16.0″/E059°27′42.7″). (c) Fault measurements (equal area lower hemisphere projection) at same location as Figure 3b. Arrows indicate movement direction of hanging wall. Compiled with FaultKin 5 [*Marrett and Allmendinger*, 1990].

Granites, typically with porphyric texture and pink orange weathering color, crop out as variously sized bodies (tens to hundreds of meters) between Remeshk and Mokhtaramabad (Figures 2 and 4c). They intruded into a light gray, thickly bedded recrystallized limestone and shales (Figure 4d). The shallow water fauna ascribes these limestones to Jurassic shelf deposits [*McCall et al.*, 1985]. Granite at the limestone-granite contact often has a fine-grained texture interpreted as chilled margin.

The two main granitoid outcrops are a west-east elongated, 30 km long and 2 km wide diorite body along the northern border of the Dur Kan Complex and a 30 km × 3 km trondhjemite body to the south of the diorite (Figure 4e). Decimeter- to meter-thick trondhjemite dikes and millimeter- to centimeter-thick plagioclase veins within the southern border of the diorite body demonstrate intrusion of trondhjemite into diorite (Figure 4f). In some places, trondhjemite/diorite contacts are burgeoning, which along with the absence of a chilled margin, suggests that diorite was incompletely crystallized when trondhjemite intruded (Figure 4g). Plagiogranite occurs on top of the granitoid intrusions or as dikes cutting them. All granitoids are in turn covered by diabase and lava and, in some places, cut by meter-thick diabase dikes (Figure 4h). These dikes swarm out from a main diabase body about 15 km west of Kotij (Figure 2) and cut all types of granitoids. Diabase, also covered unconformably by doleritic lava flows, is mostly restricted to the area around Kotij. The conformably covering doleritic lavas are related to the diabase because they show a gradual contact, similar textures, and phenocrysts. In some places, brown to red basaltic pillow lavas and nonpillowed flows unconformably cover diabase along a strongly altered zone, interpreted as paleosurface. The angular relationship (~20°) between magmatic foliation in diabase and "bedding" of pillow lava, which are interlayered with Valanginian sediments [*McCall et al.*, 1985], marks the unconformity, which further indicates that diabase and associated doleritic lavas were exposed on the seafloor when pillow lavas erupted. These structural relationships indicate that granites constitute the oldest igneous rocks and were successively intruded by a suite of diorite, trondhjemite, and plagiogranite followed by diabase. Unconformable lavas and sediments bound their age as older than 139 Ma. All lavas described in this study are part of the Valanginian sequence.

3. Petrography

The diorite, trondhjemite, plagiogranite, granite [*Streckeisen*, 1976], diabase, and lava have been studied under the optical microscope to define mineralogy, textural relationships, and to choose representative samples (locations in Figure 2 and Appendix Table S1 in the supporting information) for geochemical analysis.

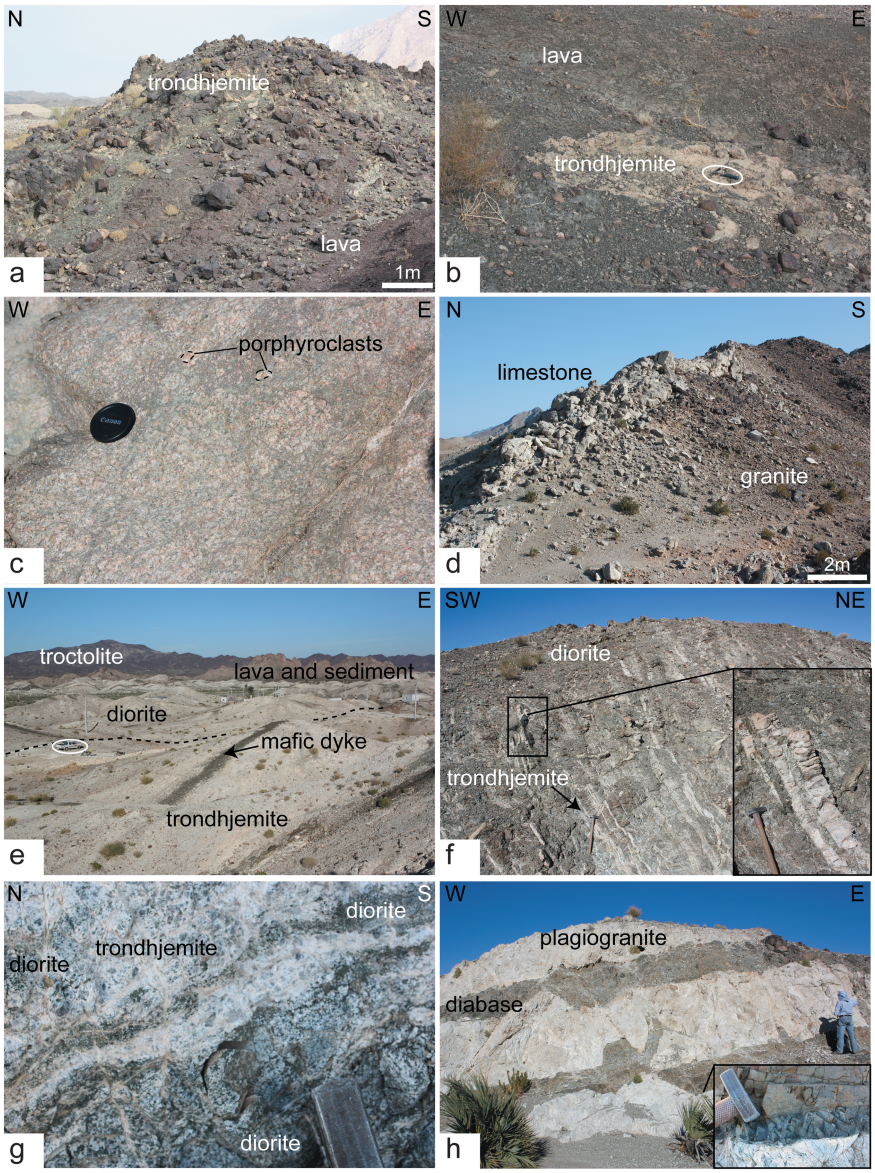

Figure 4. Field aspect and relationships between the studied North Makran granitoids. (a) Trondhjemite below lava (26°37′34.6″N/59°52′57.3″E). (b) Trondhjemite enclaves in lava (26°43′16.5″N/58°58′10.8″E). (c) Granite (26°43′48.7″N/58°51′05.6″E). (d) Recrystallized limestone on granite (26°43′52.7″N/58°51′25.0″E). (e) Diorite and trondhjemite, cut by diabase dikes, beneath lavas and sediments (26°43′35.1″N/58°56′05.1″E). (f) Dykes and veins of trondhjemite in diorite (26°46′43.5″N/58°49′49.3″E). (g) Wavy and interdigitating contact between trondhjemite veins in diorite 10 km south of Remeshk (26°46′01.4″N/58°51′02.0″E). (h) East-west trending mafic dikes (Mak-10-44) cutting trondhjemite and plagiogranite (Mak-10-45) (26°43′52.5″N/58°56′02.1″E). The close up shows the chilled margin of dike.

3.1. Granite

Granite is holocrystalline and has locally a foliated porphyric texture. Euhedral to subhedral K-feldspar phanerocrysts (<3 mm; Figure 4c) with straight grain boundaries and braided lamellae with perthitic texture (Figure 5a) constitute ~40% of the rock. The fine-grained matrix (<0.1 mm) is mostly composed of plagioclase (~35%) and quartz (~20%). Biotite (~3%), accessory phase accessories, mostly ilmenite and hematite, forms the rest of the rock. Intergrown quartz and feldspar display granophyric and micrographic textures. These features characterize eutectic crystallization of quartz and plagioclase from a high silica melt. Such textures are associated with relatively rapid cooling of silicate liquid [*Dunham*, 1965] as it is often found in A-type granites intruding colder crust in a continental rift environment [*Coleman et al.*, 1992].

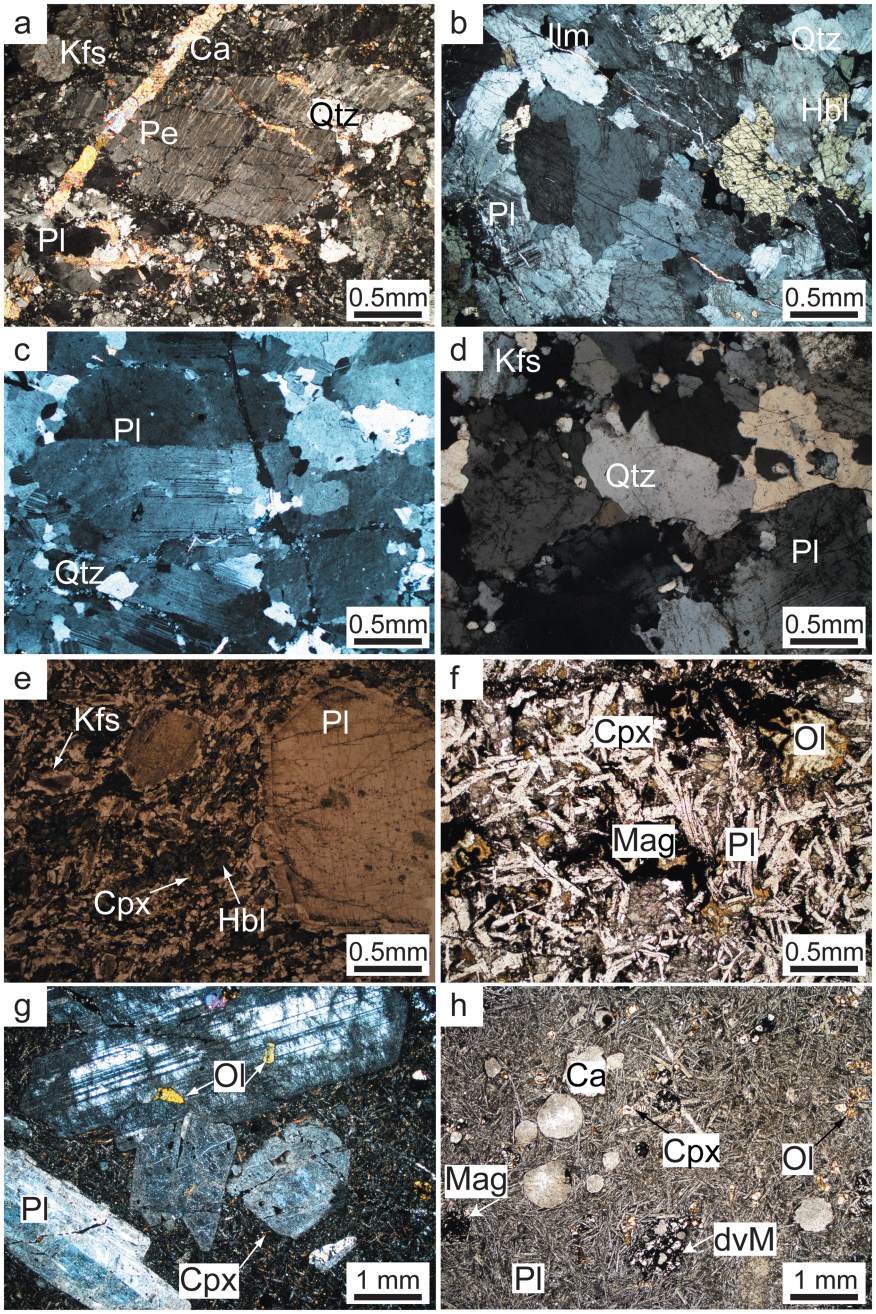

Figure 5. Photomicrographs of the North Makran granitoids and volcanic rocks. Mineral abbreviations after [*Kretz*, 1983; *Whitney and Evans*, 2010], except dvM = devitrified melt and Pe = perthite. (a) Granite Mak-11-37 under polarized light with perthitic exsolution texture in feldspars. (b) Diorite Mak-11-47 under polarized light with burgeoning grain boundaries between feldspar, quartz, and hornblende. (c) Trondhjemite Mak-11-32 under polarized light displaying coarse plagioclase with polysynthetic twinning, irregular grain boundaries, and consertal intergrowth between mineral grains. (d) Plagiogranite Mak-10-38 under polarized light showing interdigitating grain boundaries between feldspar and quartz; plagioclase shows polysynthetic twinning. (e) Euhedral plagioclase xenocrysts in the finer-grained matrix of diabase dike Mak-10-44 under transmitted light. (f) Lava Mak-11-35 under transmitted light with accumulations of devitrified melt, magnetite, and altered olivine in a matrix of mostly plagioclase laths. Clinopyroxene is interstitial to plagioclase. (g) Lava Mak-11-36 under transmitted light with olivine inclusions in large plagioclase phenocrysts. (h) Vesicular lava Mak-11-55 under transmitted light with dark glass and clinopyroxene accumulation and olivine in the matrix.

Biotite, often altered to chlorite, occurs in aggregates. Epidote is secondary, replacing feldspar and mica. Calcite veins are late brittle fractures.

3.2. Diorite

Diorite is holocrystalline and mostly equigranular with grain size between 0.5 mm and 1 mm. The white weathering color is due to abundant plagioclase (~70%), which shows straight or pinched out polysynthetic twinning in thin sections. Hornblende, the second most abundant mineral (~15% of the rock volume), occurs as green to brown green crystals. Quartz and K-feldspar generally occur in equal proportions (~5%). Ilmenite is the main accessory mineral (~3%) and is often associated with hornblende. Diorite has a granular texture with interdigitating grain boundaries between feldspar, quartz, and hornblende (Figure 5b). Most crystals are anhedral and display consertal intergrowth textures. Modal variations of plagioclase and quartz (0–10%), associated with variable plagioclase anorthite content, classify these rocks from diorite to quartz diorite. Some diorites show sericitization and albitization of plagioclase (Figure 5b).

3.3. Trondhjemite

Trondhjemite is holocrystalline with a porphyric texture composed of plagioclase phanerocrysts (<3 mm) surrounded by a finer-grained matrix of plagioclase, minor K-feldspar (~0.5 mm), and quartz (~0.2 mm). Plagioclase makes ~90% of the rock; other minerals are 3–5% of each K-feldspar and quartz and accessories such as ilmenite and hematite. Plagioclase phanerocrysts are subhedral and show polysynthetic twinning. Plagioclase, K-feldspar, and quartz in the matrix are anhedral. Grain boundaries are irregular and exhibit consertal intergrowth textures (Figure 5c). Finer-grained quartz occupies interstitial spaces between feldspars and often shows undulose extinction. Trondhjemite enclaves in lava contain epidote, tremolite, and albite as alteration products (Figure 4a).

3.4. Plagiogranite

Plagiogranites look like trondhjemites in the field and differ mainly in being richer in quartz and K-feldspar. Plagiogranite is holocrystalline, porphyric with plagioclase phanerocrysts (~2 mm) within a finer matrix of feldspars and quartz. The main rock-forming minerals are plagioclase (~75%), quartz (~10%), and K-feldspar (~10%). Accessory minerals are ilmenite and hematite. Plagioclase phanerocrysts are mostly subhedral and often show polysynthetic twinning. The matrix grains are anhedral with interdigitating grain boundaries defining a consertal intergrowth texture (Figure 5d). Quartz grains are rounded, interstitial with undulose extinction. Plagioclase is altered to epidote, prehnite, and albitized along contacts.

3.5. Diabase

Diabase is holocrystalline and contains plagioclase phenocrysts (<5 mm) near granitoids and in the dikes and otherwise has a typical fine-grained subvolcanic texture. Diabase consists of a framework (~50%) of lath-shaped plagioclase crystals (<3 mm long) with interstitial subhedral clinopyroxene (35%) and amphiboles (5%) with straight grain boundaries. Plagioclase phenocrysts with polysynthetic twinning are euhedral and have a more albitic rim with no straight grain boundary toward the matrix (Figure 5e). Plagioclase was the first phase crystallized. Ilmenite and magnetite are the main accessory minerals (~10%). They often are intergrown with amphibole and pyroxene in a skeletal texture. Diabase is usually well preserved, but in some places, epidote and occasionally chlorite replace plagioclase, and tremolite or actinolite replace clinopyroxene. Green to green brown hornblende and plagioclase are the main components of the dikes, while K-feldspar and minor amounts of clinopyroxene occur within the matrix. Doleritic lavas correspond to diabase but are slightly finer grained.

3.6. Lavas

Lavas have variable grain sizes and textures and are variably altered. The most common type, which has been attributed to Valanginian sediments, is dark brown to black, fine grained, and hypocrystalline. Lath-shaped (<0.5 mm long) plagioclase is the main rock-forming mineral (~60%). Some lavas are porphyric with larger plagioclase phenocrysts (<1 cm) in a fine red groundmass of mostly plagioclase, magnetite, clinopyroxene, glass, and larger olivine crystals (~2 mm; Figure 5g). Plagioclase phenocrysts are euhedral, whereas matrix plagioclase is fibrous, often in radial clusters. Grains of altered olivine reach up to 0.5 mm in size (Figure 5f). Clinopyroxene grains <0.5 mm are interstitial between plagioclase. The groundmass is cryptocrystalline and often devitrified dark brown glass. Magnetite is the main accessory mineral, commonly symplectitic with

AGU Tectonics

10.1002/2014TC003768

Table 1. Description of Zircons and Age Groups of Granitoids

		Inherited Zircons and Cores			Magmatic Zircons			Recrystallized or Altered Zircons		
Sample	Method	Morphology and Texture	Size (μm)	Age (Ma)	Morphology and Texture	Size (μm)	Age (Ma)	Morphology and Texture	Size (μm)	Age (Ma)
Granite										
Mak-11-37	SHRIMP	-	-	-	euhedral, oscillatory zoning	120–300	176.0 ± 0.9	-	-	-
Mak-11-57	SHRIMP	-	-	-	euhedral, oscillatory zoning	120–300	170.0 ± 1.0	-	-	-
Diorite										
Mak-11-18	SHRIMP	-	-	-	euhedral, oscillatory zoning	>200	161.3 ± 1.7	-	-	-
Mak-11-18	LA-ICP-MS	dark, euhedral, oscillatory zoning	~100	168–188, peak 170–174	euhedral, oscillatory zoning	>200	163.3 ± 0.8	-	-	-
Mak-11-47	LA-ICP-MS	dark, euhedral, oscillatory zoning	~100	165–175, peak 170	oscillatory zoning, apatite inclusions	<250	160.3 ± 0.8	bright growth zones cutting zonation	5–60	146–153
Mak-10-16	SHRIMP	dark, euhedral, oscillatory zoning	~100	~170	euhedral, oscillatory zoning	~100	165.6 ± 1.7	-	-	-
Trondhjemite										
Mak-09-194	SHRIMP	bright core	150–250	~174	euhedral, oscillatory zoning	150–250	160.5 ± 1.4	-	-	-
Mak-09-263	LA-ICP-MS	small dark grains and cores	<150	165–175	euhedral, oscillatory zoning	250	158.7 ± 1.3	rims and bright growth zones cutting zonation	5–50	144–153
Mak-11-32	LA-ICP-MS	small dark grains and cores	~150	164–186	euhedral, oscillatory zoning	250	159.7 ± 0.7	rims	~40	154–156
Plagiogranite										
Mak-10-38	SHRIMP	small dark grains and cores	~100	~165	euhedral, oscillatory zoning	150–250	156.5 ± 1.7	-	-	-
Mak-10-45	SHRIMP	darker cores	~250	162–167	euhedral, oscillatory zoning	~200	153.4 ± 2.2	rims and bright growth zones cutting zonation	50	134–145

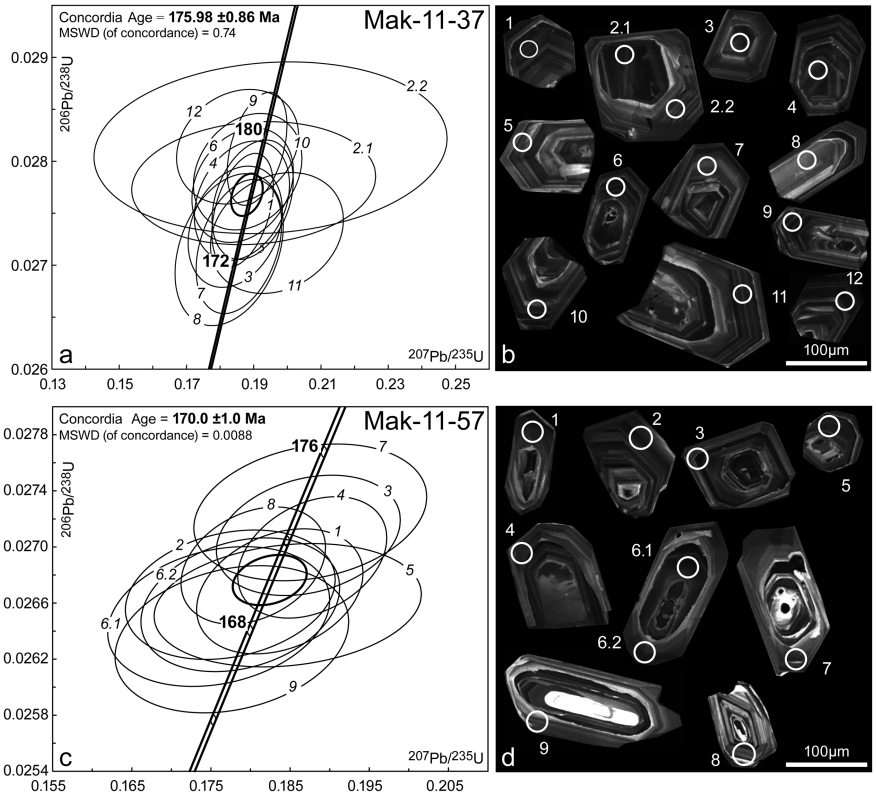

Figure 6. Sensitive high-resolution ion microprobe (SHRIMP) U-Pb zircon ages of the North Makran granite. Data-point error ellipses in Concordia diagrams are 2σ, decay-constant errors included. SHRIMP data are given in Appendix Table S2 in the supporting information. (a) U-Pb Concordia diagram and (b) CL images of measured spots on zircons of Mak-11-37. (c) U-Pb Concordia diagram and (d) CL images of measured spots on zircons of Mak-11-57.

clinopyroxene. Vesicular pillow lavas at the upper lava levels are very fine grained and mostly consist of needle-like plagioclase, frequently in radial clusters, in the matrix of devitrified dark brown glass (Figure 5h). Clusters of clinopyroxene, amphibole, and glass reach ~1 mm within the matrix. Smaller grains (~0.1 mm) of clinopyroxene and green altered olivine are parts of the matrix. Vesicles are filled with calcite. The vesicular pillow lavas are often altered with epidote and chlorite-replacing plagioclase and tremolite-replacing clinopyroxene.

4. Geochronology

The zircon morphology, size, and crystallization ages of the analyzed samples are listed in Table 1. The methods and detailed description of zircon populations are given in Appendices Texts S1 and S2 in the supporting information, respectively.

4.1. Granites

We identified one magmatic generation of zircons in both granite samples with well-confined concordant ages (Figure 6). We therefore contend that these 176.0 ± 0.96 Ma and 170.0 ± 1.0 Ma concordant ages represent crystallization ages.

4.2. Diorites

All diorite samples have a dominant zircon population that yields concordant or intercept ages between 160.3 ± 0.8 Ma and 165.6 ± 1.7 Ma (Figure 7). These ages represent the youngest zircons in two samples (Figures 7d and 7g) and were thus interpreted as crystallization ages. All samples contain older grains and cores (170–188 Ma) coinciding with zircon ages obtained in the granites. These old fractions are interpreted as assimilated grains, xenocrysts, and inherited cores. The few young ages (148–153 Ma) observed only in diorite Mak-11-47 were obtained from bright blurry patches/growth zones or rims. This sample was taken near trondhjemite and plagiogranite intrusions, which are cut by diabase dikes. Blurry contacts, thin

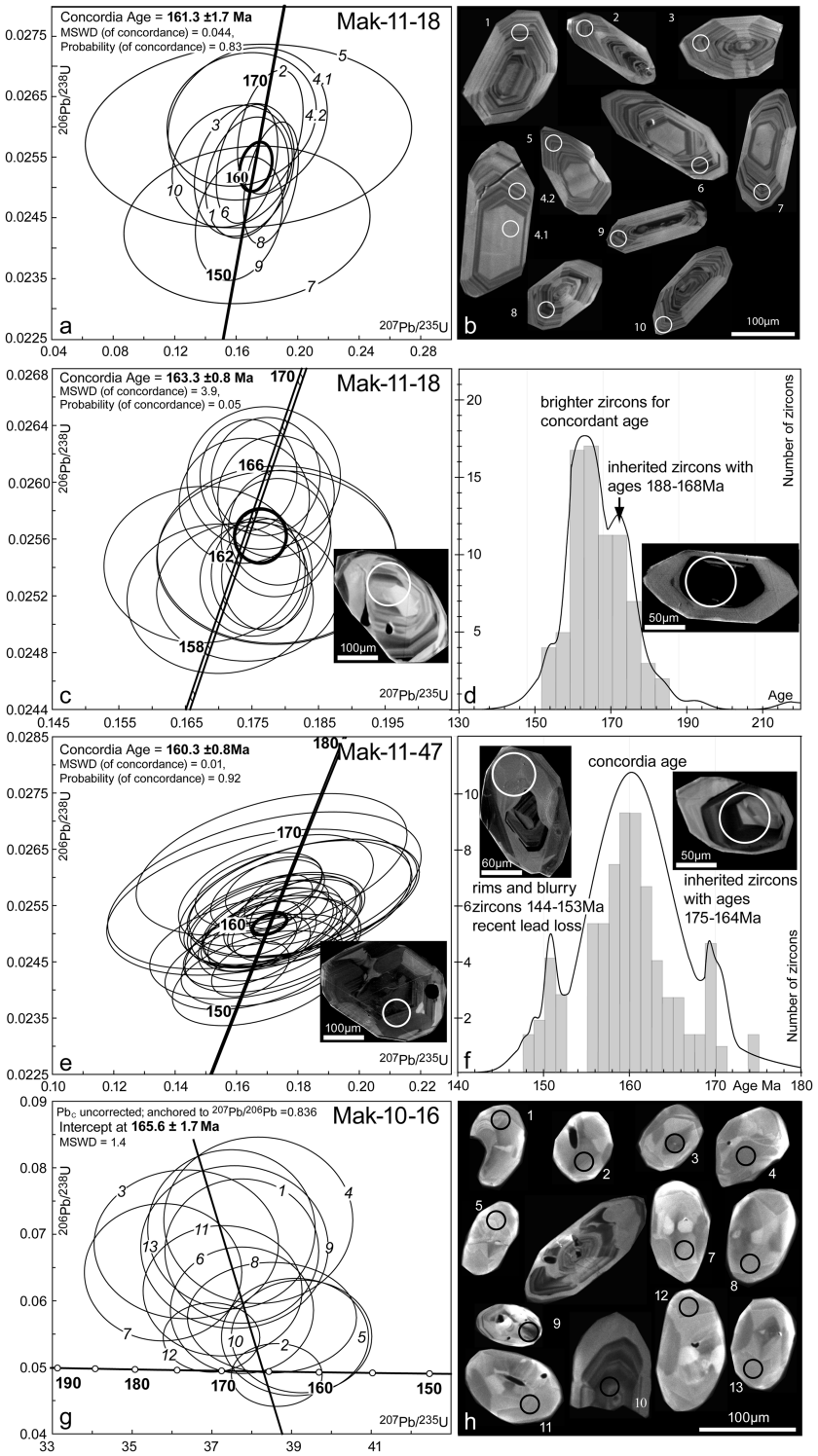

Figure 7. U-Pb zircon ages of North Makran diorites. Data-point error ellipses in Concordia diagrams are 2σ, decay-constant errors included. SHRIMP data are given in Appendix Table S2 in the supporting information and LA-ICP-MS in Appendix Table S3 in the supporting information. (a) U-Pb Concordia diagram and (b) CL images of measured spots on zircons of Mak-11-18 with SHRIMP analyses. (c) U-Pb Concordia diagram of main zircon group in sample Mak-11-18 analyzed by La-ICP-MS and (d) histogram including older core U-Pb ages and representative CL images. (e) U-Pb Concordia diagram of main zircon group in sample Mak-11-47 analyzed by La-ICP-MS and (f) histogram with U-Pb age groups of older cores and younger rims with representative CL images. (g) U-Pb Concordia diagram and (h) CL images of measured spots on zircons of Mak-10-16 with SHRIMP analyses.

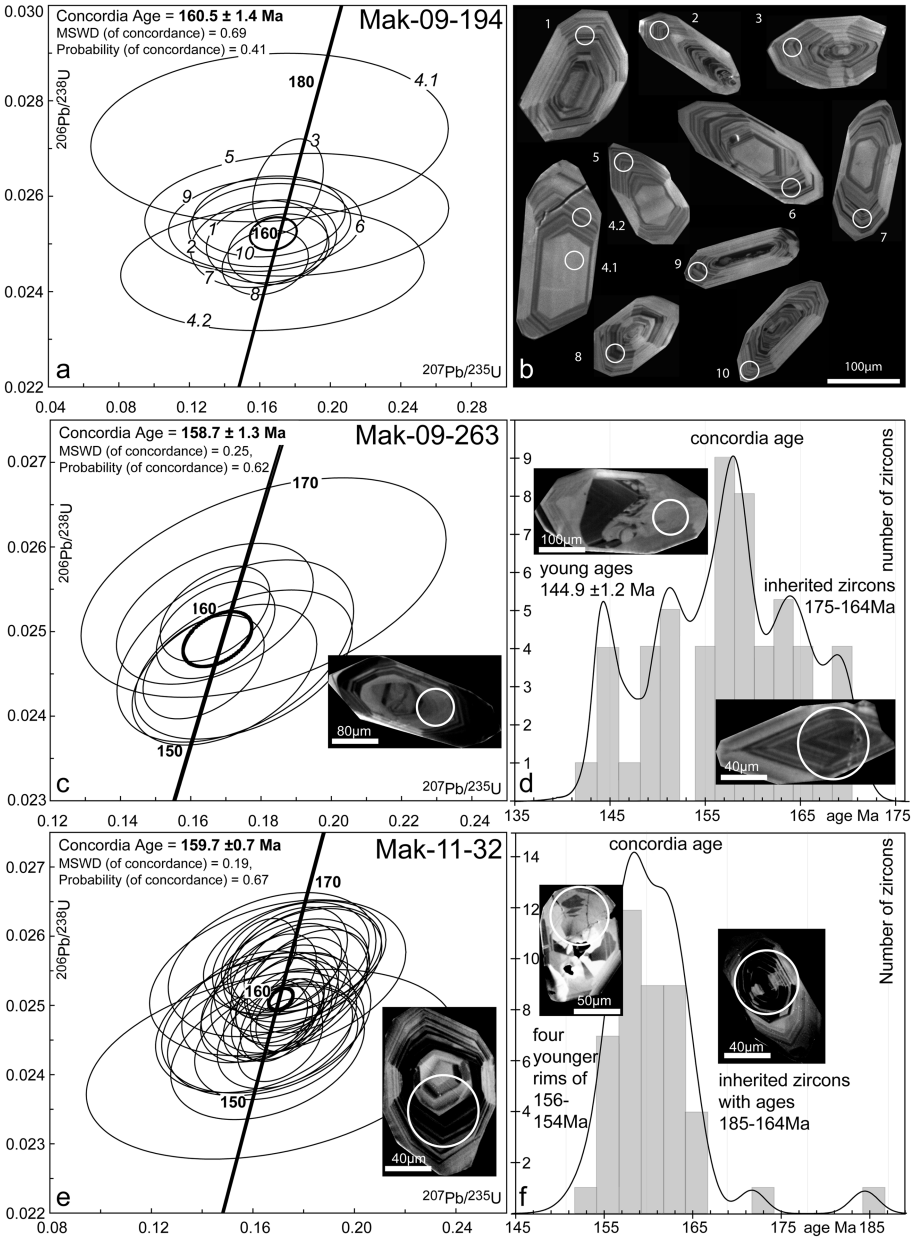

Figure 8. U-Pb zircon ages of North Makran trondhjemites. Data-point error ellipses in Concordia diagrams are 2σ, decay-constant errors included. SHRIMP data are given in Appendix Table S2 in the supporting information and LA-ICP-MS in Appendix Table S3 in the supporting information. (a) U-Pb Concordia diagram and (b) CL images of measured spots on zircons of Mak-09-194 with SHRIMP analyses. (c) U-Pb Concordia diagram of main zircon group in sample Mak-09-263 analyzed by La-ICP-MS and (d) histogram of older and younger U-Pb ages with representative CL images. (e) U-Pb Concordia diagram of main zircon group in sample Mak-11-32 analyzed by La-ICP-MS showing concordant age and (f) histogram of older and younger U-Pb ages of rims with representative CL images.

plagioclase veins in the rock, sericitization, and albitization of plagioclase indicate hydrothermal alteration. The interpretation of these younger ages will be discussed in section 4.6.

4.3. Trondhjemites

All trondhjemite samples have a dominant zircon generation with concordant ages between 158.7 ± 1.3 Ma and 160.5 ± 1.4 Ma (Figure 8). Since they represent the generally most abundant and youngest zircons in two of the three samples, these concordant ages were interpreted as crystallization ages. Older cores and few grains yielded ages from 163 to 186 Ma, which are consistent with crystallization ages of diorites and granites.

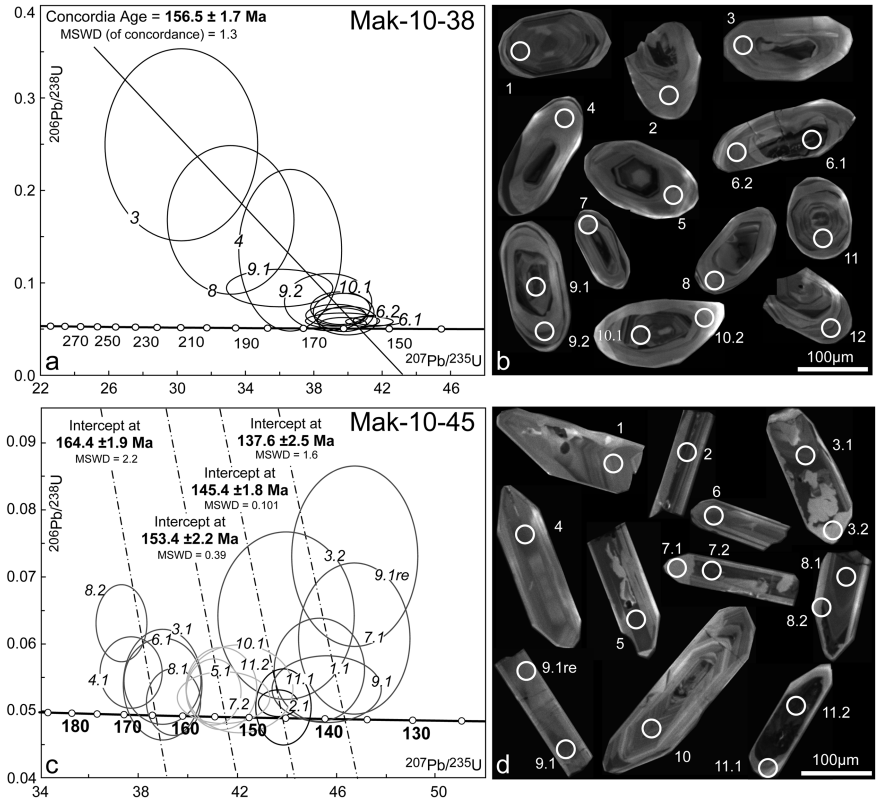

Figure 9. SHRIMP U-Pb zircon ages of the North Makran plagiogranites. Data-point error ellipses in Concordia diagrams are 2σ, decay-constant errors included. SHRIMP data are given in Appendix Table S2 in the supporting information. (a) U-Pb Concordia diagram and (b) CL images of measured spots on zircons of Mak-10-38. (c) U-Pb Concordia diagram and (d) CL images of measured spots on zircons of Mak-10-45.

These zircons are thus interpreted as assimilated grains and inherited cores. The 144–156 Ma ages in sample Mak-09-263, a few meters long trondhjemite enclave in Valanginian lava [*Dolati*, 2010], are similar to those found in diorite sample Mak-11-47 and will also be discussed in section 4.6.

4.4. Plagiogranites

Plagiogranite samples show multiple zircon age groups (Figure 9). The intercept age 156.5 ± 1.7 Ma of Mak-10-38 is considered to be the crystallization age (Figure 9a). The youngest 141 ± 1.5 Ma age (Figure 9b, zircon 6.1) was measured in a zircon core, whereas the rim yields an age of 166.9 ± 6.2 Ma (Figure 9b, zircon 6.2). This suggests that the ages off the intercept line likely feature lead loss. Sample Mak-10-45 is more complex regarding zircon morphology and age distribution (Figure 9c). There is an obvious correlation between zircon's age and their width/length ratio. Zircons with small shape ratios (e.g., Figure 9d; Mak-10-45_2, 7, 9), usually attributed to rapid cooling and fast crystallization, have ages <153 Ma. We interpreted the intercept at 153.4 ± 2.2 Ma to be the intrusion age because it is measured in a core of a small thin zircon (Figure 9d; Mak-10-45_7.2) and in outer zones of bigger grains with core ages of ~160 Ma (Figure 9d; Mak-10-45_3.1). The older ages represent zircons inherited from diorite and trondhjemite. These inherited grains have a bigger width/length ratio, which suggests a slower crystallization environment than the younger zircons. The two youngest intercept ages of 145.4 ± 1.8 Ma and 137.6 ± 2.5 Ma (Figure 9c) will be addressed in section 4.6.

4.5. Age Constraints for Diabase and Lava

No zircon was found in crushed samples of diabase and lavas of the Dur Kan Complex. Chilled margins of the dikes (Mak-10-44) cutting plagiogranite show that diabase intruded into an already crystallized plagiogranite and thus indicate ages <153 Ma. The overlying lavas are interlayered with fossiliferous Valanginian (140–133 Ma) [*International Chronostratigraphic Chart 2014/02,* 2014] sediments [*McCall et al.*, 1985]. This suggests that

Table 2. Sr-Nd Isotopic Analyses of Representative Rocks From the Northern Part of the Dur Kan Complex[a]

Rock Type	Sample	Rb (ppm)	Sr (ppm)	$^{87}Rb/^{86}Sr$	$^{87}Sr/^{86}Sr$	±2σ% rel.	$(^{87}Sr/^{86}Sr)_{in}$	Rock Age	Sm (ppm)	Nd (ppm)	$^{147}Sm/^{144}Nd$	$(^{143}Nd/^{144}Nd)$	±2σ% rel.	$(^{143}Nd/^{144}Nd)_{in}$	ε_{Nd}	$\varepsilon_{Nd(i)}$
Granite	Mak-11-57	19.2	104.7	0.518674	0.707260	0.000011	0.706006	170 Ma	2.4	13.1	0.114921	0.512339	0.000004	0.512211	−5.8	−4.1
	Mak-11-45	26.8	70.8	1.069159	0.709113	0.000009	0.706529	~170 Ma	5.0	20.0	0.157977	0.512561	0.000004	0.512385	−1.5	−0.7
Diorite	Mak-10-37	0.4	711.8	0.001389	0.704319	0.000005	0.704316	~160 Ma	2.7	10.5	0.158928	0.512717	0.000006	0.512545	1.5	2.2
	Mak-09-247	1.2	442.2	0.007548	0.704255	0.000017	0.704238	~165 Ma	2.7	7.7	0.219287	0.512754	0.000004	0.512524	2.3	1.8
	Mak-11-47	1.0	540.7	0.005058	0.704266	0.000009	0.704254	163 Ma	1.3	4.8	0.169524	0.512701	0.000008	0.512524	1.2	1.8
Trondhjemite	Mak-11-32	0.2	336.7	0.001358	0.704841	0.000016	0.704838	159 Ma	1.1	6.5	0.110130	0.512639	0.000006	0.512524	0.0	1.8
	Mak-09-194	9.4	421.9	0.063045	0.705158	0.000008	0.705015	160 Ma	1.8	9.0	0.123449	0.512638	0.000021	0.512509	0.0	1.5
Plagiogranite	Mak-10-38	0.0	293.1	0.000211	0.704671	0.000003	0.704671	156 Ma	0.1	0.9	0.095736	0.512641	0.000007	0.512543	0.1	2.1
	Mak-10-45	3.3	558.4	0.016667	0.704207	0.000021	0.704173	153 Ma	0.3	1.8	0.097057	0.512665	0.000023	0.512568	0.5	2.5
Diabase	Mak-10-44	12.3	314.0	0.110129	0.704212	0.000022	0.703987	~144 Ma	7.0	26.4	0.167568	0.512941	0.000005	0.512783	5.9	6.4
Lava	Mak-11-36	17.0	242.9	0.198040	0.704081	0.000006	0.703687	~140 Ma	5.4	23.3	0.145007	0.512935	0.000004	0.512802	5.8	6.7
	Mak-11-35	2.4	133.7	0.050571	0.704197	0.000021	0.704096	~140 Ma	3.4	12.5	0.171194	0.512937	0.000004	0.512780	5.8	6.3
	Mak-11-55	1.8	292.0	0.017011	0.703702	0.000019	0.703668	~140 Ma	3.3	11.4	0.183242	0.512936	0.000009	0.512768	5.8	6.1
	Mak-10-100	10.9	380.5	0.080555	0.705156	0.000018	0.704996	~140 Ma	9.5	41.5	0.144243	0.512867	0.000002	0.512735	4.5	5.4

[a]Chrondritic reservoir values $^{87}Rb/^{86}Sr = 0.0847$, $^{87}Sr/^{86}Sr = 0.7047$, $^{147}Sm/^{144}Nd = 0.1967$, $^{43}Nd/^{144}Nd = 0.512638$ [*Jacobsen and Wasserburg*, 1984]. Errors are in percent relative at 2σ.

diabase and associated doleritic lava are Valanginian or older. Using these constraints, we took 140 Ma as reference age to calculate the isotopic ratios of diabase and lavas.

4.6. Discussion of the Young Ages

The young U-Pb ages with peaks at ~145 Ma in samples Mak-11-47, Mak-09-263, and Mak-10-45 were measured only in few zircons. These zircons show a texture that differs significantly from the typically magmatic oscillatory zoning of the older groups (crystallization age and inherited grains/cores). This texture is, in most cases, a brighter cathodoluminescence (CL) growth zone with no magmatic growth rims cutting oscillatory zoning and cores. Such features are not consistent with an igneous origin and typically denote a recrystallization event [e.g., *Vavra*, 1990; *Pidgeon*, 1992; *Hoskin and Schaltegger*, 2003; *Puga et al.*, 2005]. Very rarely (four grains in all three samples), young ages occur in small (<60 μm) zircons, with no oscillatory zoning. We contend that lead loss, which can erase growth rings and produce young ages in nonabraded grains [e.g., *Krogh*, 1982; *Pidgeon*, 1992; *Mattinson*, 2005], caused this texture. Pressure release or minor heating events, such as the emplacement of lava, can cause both recrystallization and lead loss in contact zones.

Supporting explanation for these young ages not being crystallization ages is gained from linking field observation and zircon morphology. All samples with young ages were taken near the contact to diabase intrusions or doleritic lava flows, which are as old as or older than the overlying Valanginian (140–133 Ma) [*McCall et al.*, 1985] sequence. Concordant ages and peaks of young zircons peak around 145 Ma, which could well represent the age of diabase and doleritic lavas. These magmatic rocks are widespread, thus represent an extensive event that may be responsible for lead loss and even zircon recrystallization close to the contact with hot magma. Since there is no other magmatic or deformation event in the region within that time frame, we suggest that diabase intrusion and effusion of doleritic lava are responsible for the zircon recrystallization and lead loss at ~145 Ma.

5. Geochemistry

Twenty-two representative samples, including 2 granites, 7 diorites, 3 trondhjemites, 2 plagiogranites, 2 diabases, and 2 lavas, were used to discuss major, minor, and trace element geochemistry. Results are given in Appendix Table S4 in the

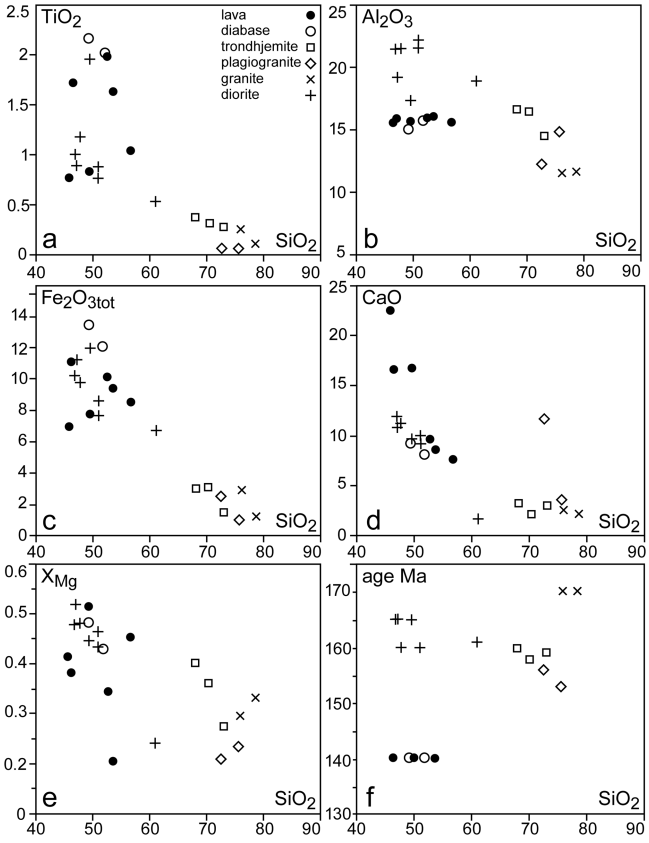

Figure 10. Variation diagrams of North Makran granitoid and lava bulk compositions with SiO_2 versus (a) TiO_2, (b) Al_2O_3, (c) Fe_2O_3tot, (d) CaO, (e) X_{Mg}, and (f) age. Data are given in Appendix Table S4 in the supporting information.

supporting information. Sixteen out of the 22 representative powdered bulk samples were also analyzed for Sr and Nd isotopes at ETH Zürich. The results are listed in (Table 2). The methods used for bulk element and isotope analysis are described in Appendix Text S1 in the supporting information.

5.1. Granite

The granite samples have SiO_2 values clustered around of 74–77 wt % (Figure 10) with low X_{Mg} [Mg/(Fe_{tot} + Mg)] between 0.29 and 0.33. TiO_2 content is low (0.11–0.25 wt %; Figure 10a) as are Cu, Ni, and Cr. Granites have higher K_2O contents (>1.16 wt %) than the other granitoids. Granites have 10–100 times chondrite rare earth element (REE) concentrations and display enrichment in light rare earth elements (LREE) with respect to middle REE (MREE) and heavy REE (HREE) that lie rather flat (Figure 11a). Granites yield negative Nb, Ta, Eu, and Sr anomalies and show enriched large-ion lithophile element (LILE) concentrations. Sample Mak-11-45 (Figure 11b) has a negative Ti anomaly reflecting ilmenite fractionation; the other granite (Mak-11-57; Figure 11b) shows Ti enrichment due to ilmenite accumulation. Initial strontium isotopic ratios ($^{87}Sr/^{86}Sr_{(i)}$) of granites (Table 2) are between 0.706006(11) and 0.706529(9) (Figure 12a). Granites also display the lowest initial neodymium isotopic ratios ($^{143}Nd/^{144}Nd_{(i)}$), ranging from 0.512211(4) to 0.512385(4) (Figure 12a) with $\varepsilon_{Nd(i)}$ from −4.1 to −0.7.

5.2. Diorite

Diorites have SiO_2 contents between 46 and 50 wt % except for sample Mak-11-18 which has ~60 wt % (Figure 10). There is a positive correlation between TiO_2, Fe_2O_3, and CaO with SiO_2. Diorites have X_{Mg} between 0.43 and 0.52, again with the exception of Mak-11-18, which has X_{Mg}~0.24. Diorites have about 4–10 times chondrite REE concentrations, a concave REE pattern with a slightly positive LREE slope and negative MREE to HREE segment. N-mid-ocean ridge basalt (MORB)-normalized spider diagrams (Figure 11b) show a varying LILE section and Nb-Ta depletion. Eu, Pb, Sr, and Ti show positive anomalies. Diorites are quite uniform, except sample Mak-11-18, which has a convex REE pattern. This sample is quartz rich and close to syenite in composition. Diorite samples show a narrow range in isotopic compositions (Figure 12a), with similar $^{87}Sr/^{86}Sr_{(i)}$ (0.704238(17)–0.704316(5)) and $^{143}Nd/^{144}Nd_{(i)}$ (0.512524(8)–0.512545(6)) ($1.8 < \varepsilon_{Nd(i)} < 2.2$).

5.3. Trondhjemite

Trondhjemites have high SiO_2 compositions (>66 wt %) negatively correlated with TiO_2, Al_2O_3, and Fe_2O_3tot (Figure 10). TiO_2 is lower than in diorites, between 0.27 and 0.37 wt %. Trondhjemites have 3–40 times chondrite concentration. They show LREE enrichment relative to MREE and HREE. Like granites, they have an enriched LILE section and display a negative Nb-Ta anomaly (Figure 11b). Small positive Eu and Sr anomalies account for plagioclase accumulation. Ti is slightly enriched compared to N-MORB. Their isotopic composition lies between those of diorite and granites (Figure 12a), with $^{87}Sr/^{86}Sr_{(i)}$ ranging from 0.704838(16) to 0.705015(8) and $^{143}Nd/^{144}Nd_{(i)}$ ranging from 0.512524(6) to 0.512509(21) ($1.5 < \varepsilon_{Nd(i)} < 1.8$).

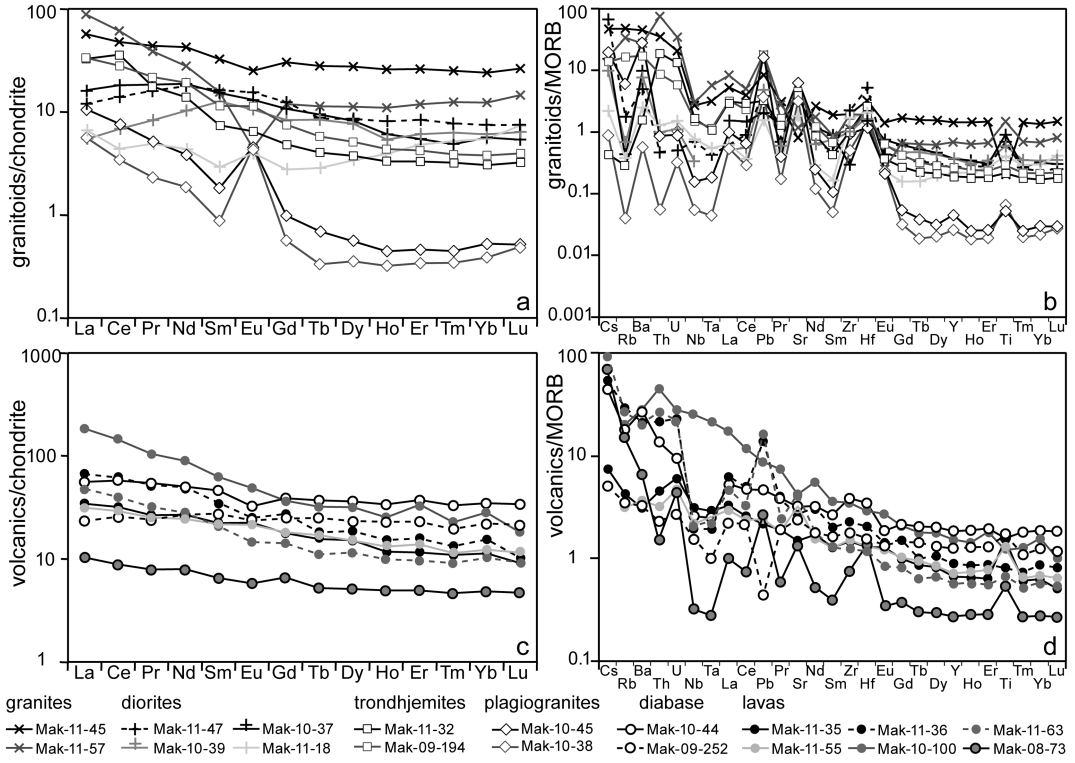

Figure 11. Trace element normalized to chondrite and N-MORB [*Sun and McDonough*, 1989]. (a) Chondrite-normalized and (b) N-MORB-normalized trace element concentrations of the North Makran granitoids. (c) Chondrite-normalized and (d) N-MORB-normalized trace element concentrations of the volcanic rocks covering the North Makran granitoids. Data are given in Appendix Table S4 in the supporting information.

5.4. Plagiogranite

Plagiogranites contain more SiO_2 (>70 wt %) than trondhjemites, but both follow the same linear trend in variation diagrams (Figure 10). The two analyzed plagiogranite samples have very low TiO_2 values (~0.07 wt %) and X_{Mg} below 0.23, 1–10 times chondrite compositions, and thus lower trace element concentrations than the other granitoids. LREE are enriched with respect to MREE and HREE (Figure 11a). Both LREE and MREE have a negative slope, while the HREE section is mostly flat. Strongly positive Eu and Sr anomalies reflect plagioclase accumulation. Positive Pb and Ti and negative Nb-Ta anomalies are similar yet more pronounced than in the other rocks (Figure 11b). The $^{87}Sr/^{86}Sr_{(i)}$ ranges between 0.704173(21) and 0.704671(3), similar to the diorite and trondhjemite composition. The $^{143}Nd/^{144}Nd_{(i)}$ ranges between 0.512543(7) and 0.512568(23) (Figure 12a), so that $\varepsilon_{Nd(i)}$ lies between 2.1 and 2.5.

5.5. Diabase and Lavas

Diabase and lava have basalt to trachyandesite compositions (Figure 13a) and belong to an alkaline series with $Na_2O + K_2O$ ranging from 4.1 to 8.2 wt %. These rocks have a higher TiO_2 content than all previously described samples (Figure 10a) and Al_2O_3 around 15 wt % (Figure 10b). Their X_{Mg} ranges from 0.21 to 0.51, indicating that they do not represent primitive mantle melts (Figure 10e) but differentiated products. Diabases have 30–60 times chondrite REE concentrations with a generally flat pattern (Figure 11c). Weak negative Eu and Sr anomalies indicate plagioclase fractionation in the parental magma prior to the formation of sample Mak-10-44, which also shows high LILE and negative Nb, Ta, and Ti anomalies (Figure 11d). Diabase from the main body (Mak-09-252) shows no LILE enrichment and has a positive Ti anomaly.

Lavas have a weakly negative REE section with 10–180 times chondrite concentration (Figure 11c). Lavas to the west of Fannuj have a negative Nb-Ta anomaly and have $^{87}Sr/^{86}Sr_{(i)}$ between 0.703687(6) and 0.704096(21), whereas Mak-10-100, to the east of Fannuj (Figure 2) [*Dolati*, 2010], displays no Nb-Ta anomaly and has a higher $^{87}Sr/^{86}Sr_{(i)}$ of 0.704996(18) (Figure 12a). Mak-11-35 and Mak-11-55 show small negative Eu and positive Ti

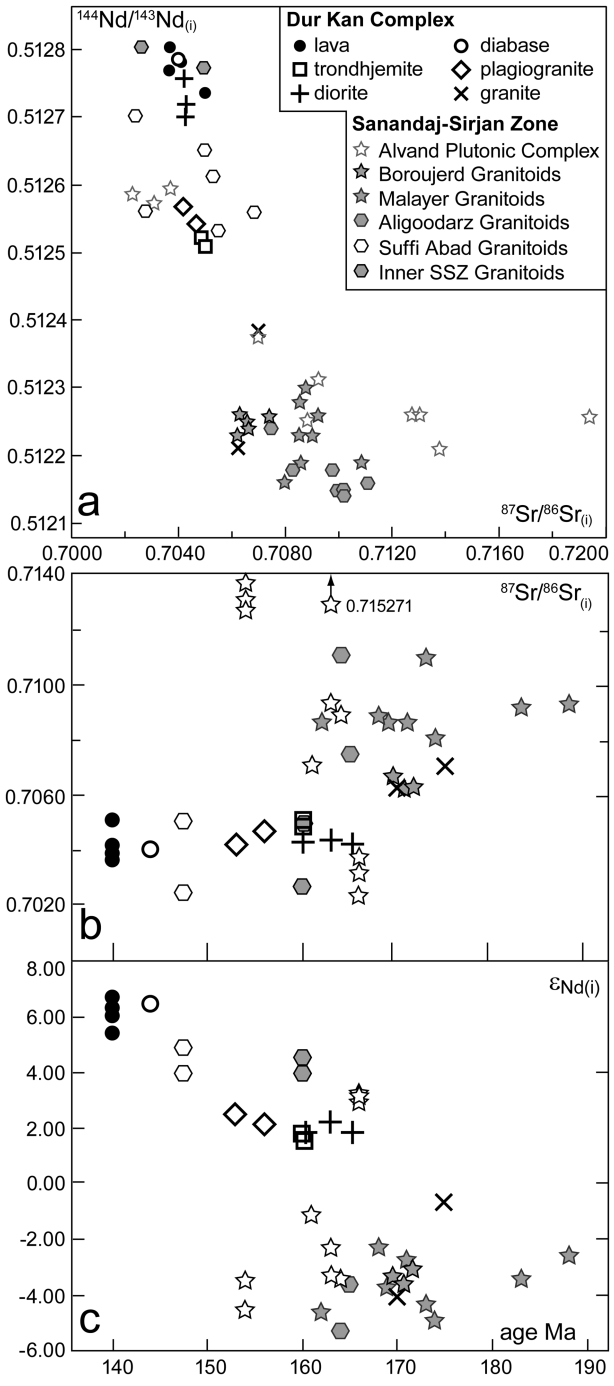

Figure 12. Isotopic compositions. (a) Initial Nd isotope ratios in function of initial Sr isotope ratios (both normalized to the corresponding crystallization age). (b) Sr isotope ratios and Epsilon Nd (both normalized to the corresponding crystallization age) in function of the age. Sanandaj/Sirjan compositions (stars in Figure 1) from the Malayer pluton [*Ahadnejad et al.*, 2011], the Boroujerd Granitoids [*Ahmadi-Khalaji et al.*, 2007], Suffi Abad granitoid [*Azizi et al.*, 2011], Aligoodarz granitoids [*Esna-Ashari et al.*, 2012], Inner Sanandaj-Sirjan Zone granitoids [*Omrani et al.*, 2008], and the Alvand Plutonic Complex [*Shahbazi et al.*, 2010].

anomalies (Figure 11d). Sample Mak-11-36 differs from the others by containing plagioclase phenocrysts in the matrix, which results in major element compositions similar to that of diabase dike Mak-10-44. It has an enriched LILE section and no Ti anomaly. The $^{143}Nd/^{144}Nd_{(i)}$ of diabase and lava lie between 0.512768(9) and 0.512802(4) ($6.1 < \varepsilon_{Nd(i)} < 6.7$; Figure 12a), with the exception of Mak-10-100 that show an $\varepsilon_{Nd(i)}$ of 5.4.

6. Discussion

The North Makran granitoids comprise minor calc-alkaline plutons and a more abundant intermediate diorite-trondhjemite-plagiogranite sequence with low-K tholeiitic affinities (Figure 13b). The North Makran granitoids are all I-type granites [*Chappell and White*, 1974], but some samples show features typical of A-type granites, such as high FeO_T/MgO and $(K_2O + Na_2O)/CaO$ and the presence of perthitic feldspar. The geochemical differences reflect different magmatic evolutions. All of these rocks are unconformably covered and intruded by alkaline diabase and lavas. The geochemical record through time allows separating three main magmatic pulses related to a progressive tectonic evolution.

6.1. Petrogenesis and Magma Sources

6.1.1. Granites: Crustal Intrusions During Continental Breakup

Granites are the oldest North Makran granitoids (Figures 11e and 11f). Unfractionated HREE and *Y* suggest that the parental melt did not fractionate in the garnet stability field. They display LREE enrichment, high large ion lithophile element (LILE) concentrations, and negative Nb and Ta anomalies, which are common in all granites involving partial melting of continental crust [*Pearce and Peate*, 1995; *Kelemen et al.*, 2003]. The North Makran granites have relatively high alkali compositions that classify them as I-type granites, although they show affinities closer to within plate granites than the other granitoids (Figures 13c and 13d). The high initial Sr isotopic ratios and negative $\varepsilon_{Nd(i)}$ are symptomatic of a significant crustal contribution to the melt

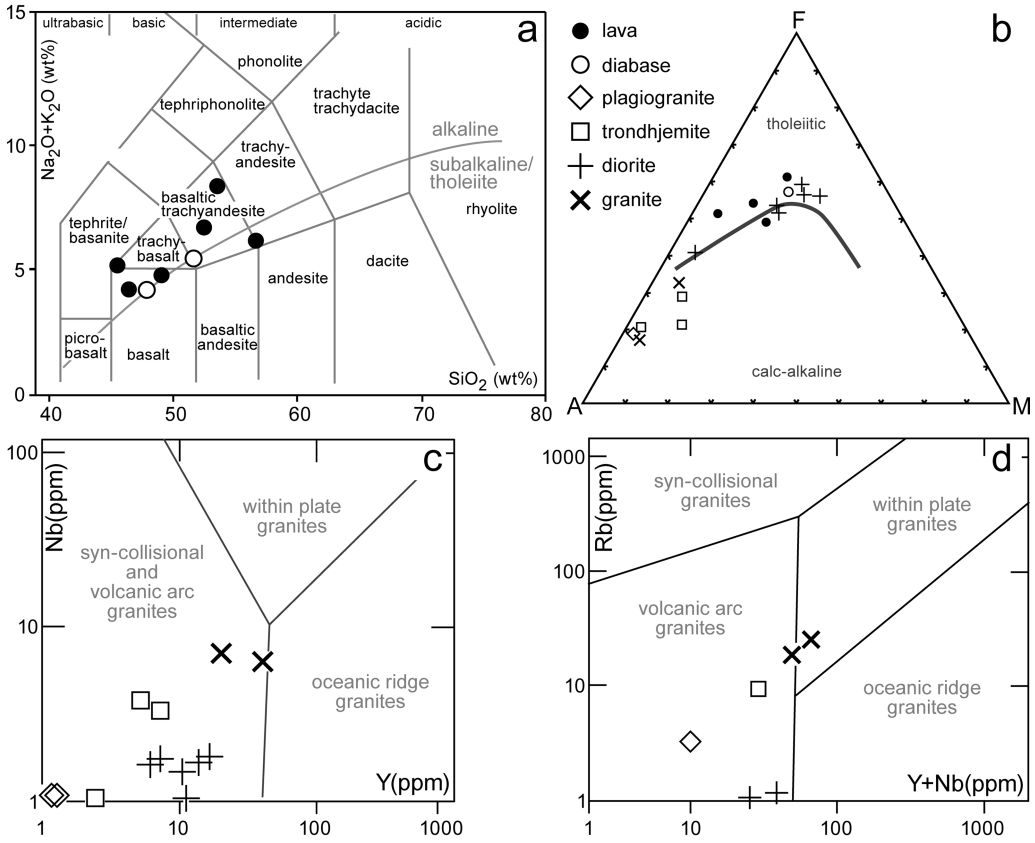

Figure 13. Geochemical classification of the studied North Makran granitoids and volcanic rocks. (a) In the Total alkali silica diagram after *Cox et al.* [1979]. Tholeiitic-calc-alkaline boundary taken from *Irvine and Baragar* [1971], (b) A = $Na_2O + K_2O$, F = FeO, and M = MgO diagram, (c) Nb/Y trace element, and (d) Rb/Y+Nb diagram after *Pearce et al.* [1984].

(Figure 12b), either inherited from the source or acquired during their petrogenesis. Interestingly, the granites show variable Nd isotopic composition for a narrow range of Sr isotopic composition, suggesting a heterogeneous source that most likely involved mafic material. Although it is difficult to disentangle the different components of the source of these granites, their overall composition would be in line with a formation via basement anatexis.

Altogether, the chemical characteristics and the petrographic textures suggest that the analyzed granites formed from a rapidly cooled calc-alkaline continentally affected magma. Granitic melts have a high viscosity and usually crystallize deep in the crust [e.g., *Pitcher*, 1979; *Johannes and Holtz*, 1991; *Clemens*, 1998]. However, the North Makran granites reached near-surface depths to intrude slightly older Middle Jurassic shelf limestones [*McCall et al.*, 1985]. Shallow emplacement and rapid cooling are further supported by the granophyric, micrographic, and perthitic textures, which are common in granite intrusions in continental rifts [*Coleman et al.*, 1992]. These observations suggest that the continental crust of the Dur Kan Complex had been considerably thinned; otherwise, the melts would have not reached the limestones of the sedimentary cover. Therefore, the granites formed during extension/thinning of a continental crust, while mantle upwelling and a subsequent high thermal gradient triggered partial melting of the basement.

6.1.2. Mixed Mantle and Crustal Melts: Diorite-Trondhjemite-Plagiogranite Suite

The diorite-trondhjemite-plagiogranite sequence displays a large range of SiO_2 content which gradually increases with younger ages of the rocks (Figure 10f). Most diorites, except Mak-11-18, have SiO_2 below 50 wt %, high X_{Mg} (>0.43), and high transition element content. This suggests higher mantle contribution than for the granites in line with the isotopic composition. Concurrently, rising SiO_2 content from diorite to plagiogranite corresponds to a decrease in X_{Mg}, TiO_2, Al_2O_3, Fe_2O_3tot, CaO, and MgO, interpreted to mark the differentiation trend from a common parental melt.

Trondhjemite and plagiogranite with $X_{Mg} < 0.40$ have much lower transitional element content than diorites and thus represent more differentiated products of the magma suite. Although the differentiation trend evolves through time (SiO_2 increases from 165 to 155 Ma; Figure 10f), the diorite-trondhjemite-plagiogranite suite has a near-constant isotopic composition with $\varepsilon_{Nd(i)}$ from 1.8 to 2.2 and $^{87}Sr/^{86}Sr_{(i)}$ between 0.704173 and 0.705015, suggesting a common magma source during the formation of these rocks (Figure 12b). The higher $^{87}Sr/^{86}Sr_{(i)}$ are directly related to rocks that are either enclaved in lava or close to an intrusion contact, hinting that reheating by the lavas and/or hydrothermal fluids, possibly on the ocean floor, altered these Sr isotopic features. The isotopic composition of the less fluid mobile Nd further indicates that the magma source has a mixed mantle and crustal component. This can be explained by assimilation of the preexisting crust (i.e., the granites) into fractionating mantle melts, therefore, explaining the presence of inherited zircons having the same ages as granites. The diorite-trondhjemite-plagiogranite sequence has compositions in accordance with a syncollisional and volcanic arc origin (Figures 13c and 13d). The diorites show no LREE enrichment, a flat HREE section, a positive Ti anomaly, and only weak Nb and Ta negative anomalies (Figures 11a and 11b). Thus, they lack features typical for subduction-related granitoids; instead, they probably are associated to a MORB-like setting. Trondhjemite and plagiogranite on the other hand show LREE enrichment and are depleted in Nb and Ta. This is interpreted as a differentiation feature since there is no isotopic evidence for a change in melt source.

6.1.3. Mantle-Derived Diabase and Lavas

The diabase and lavas have alkaline signatures and contrast with all other lithologies. The unconformable contact between lavas and underlying granitoids and the enclaves of trondhjemite within lavas requires separating the latter from the diorite-trondhjemite-plagiogranite sequence. The time gap is constrained by the 165–153 Ma zircon ages and the fossiliferous Valanginian sediments interlayered with the lavas. Normalized to N-MORB, some lavas show negative anomalies in Nb and Ta and steady enrichment from HREE to the most incompatible elements (Figures 11c and 11d). The basaltic to trachyandesitic compositions (Figure 13a), the presence of primary olivine, and high concentrations of transitional elements point toward the mantle-derived melts. Their mantle source is readily confirmed by the Sr and Nd isotopic composition that approach MORB values ($^{87}Sr/^{86}Sr_{(i)} = 703687$ to 0.704996, $\varepsilon_{Nd(i)} = 5.4$ to 6.7; Figure 12b). This alkaline suite of mantle-derived melt is consistent with the formation in a marginal basin during continental rifting and/or back-arc formation [e.g., *Pearce et al.*, 1984; *Harris et al.*, 1986; *Kelemen et al.*, 2003]. Since not all lavas have enriched LILE and a strong negative Nb and Ta anomaly, there is no robust indication of subduction influence.

6.2. Tectonic Evolution of the Dur Kan Complex

Bringing together field observations, geochemical and age constraints allow reconstructing 30 Ma of Mesozoic tectonic and magmatic evolutions (Figure 14). The Early to Middle Jurassic calc-alkaline granites (176–170 Ma) intruded into the Jurassic shelf limestone of the Iranian continental Tethys margin (Figure 14a). This structural aspect, together with the granite geochemical affinity, suggests a formation through remelting of a preexisting basement during lithospheric thinning. The Late Jurassic diorite-trondhjemite-plagiogranite suite (165–153 Ma) intruded the granites and was derived from a rather homogeneous, less radiogenic melt source with less crustal contribution. Inherited 170 and 175 Ma zircons are consistent with the Jurassic granites being part of the crustal contamination. Again, mantle upwelling and partial melting beneath a thinning continental crust may explain these characteristics (Figure 14b). The geochemistry of the diorite-trondhjemite-plagiogranite suite expresses increased mantle input into a magma chamber at shallow depth, corresponding to the observed low-pressure fractional crystallization sequence. Therefore, we suggest that the diorite-trondhjemite-plagiogranite formed through an ~10 Ma long-lived magmatic system in an extending continental margin (Figure 14b). These magmatic rocks were exhumed, possibly in horsts or tilted blocks before the lava flowed on top before the Late Valanginian. Interlayered cherts contain radiolarian specimens [*McCall et al.*, 1985] typical for a deep-sea environment. These sediments contrast with the shelf environment in which the granitoids intruded and demand deepening of the sedimentation environment. Deepening of the depositional environment coeval with exhumation of plutonic bodies is best associated with extension, which reached an "oceanic spreading"-like situation in the Early Cretaceous (Figure 14c). The magmatic response of this system is supported by the presence of the alkaline to tholeiitic suite of mantle-derived diabase and lava that crosscut all granitoids. Extension is consistent with and would be nearly orthogonal to the numerous WNW-ESE striking mafic dikes and intrusions. The increased mantle component with younging of the rocks agrees with Middle Jurassic to Early Cretaceous extension. Deepening

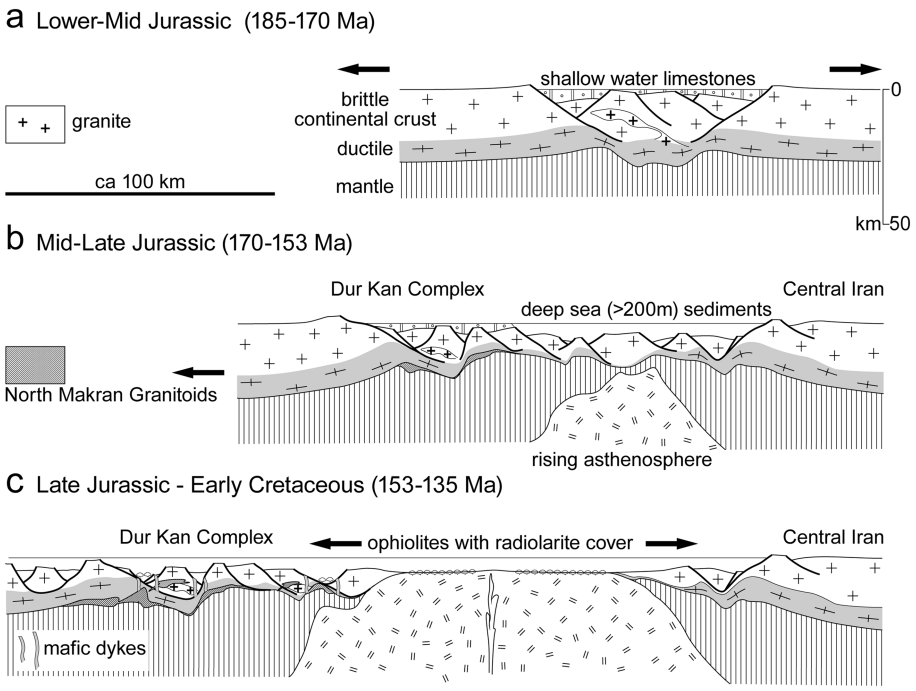

Figure 14. Sketch (not to scale) of the tectonic interpretation during the formation of the North Makran granitoids and the lava cover from Middle Jurassic to Early Cretaceous.

of the sedimentary environment from Jurassic shallow water shelf deposits to shales, limestones, and cherts in Early Cretaceous is in line with crustal thinning and consequent subsidence.

6.3. Reassessment of the North Makran Evolution

6.3.1. Dur Kan Complex: A Continuation of the Sanandaj-Sirjan Zone

Within the frame of North Makran, the intermediate plutons and younger volcanic rocks have been interpreted as the most differentiated rocks of the North Makran Ophiolites [*McCall et al.*, 1985]. New field observations and geochemical and geochronological data indicate affiliation of North Makran granitoids to those described in the Sanandaj-Sirjan Zone [e.g., *Ahmadi-Khalaji et al.*, 2007; *Shahbazi et al.*, 2010; *Ahadnejad et al.*, 2011; *Esna-Ashari et al.*, 2012]. There, 170–185 Ma old granite intrusions have Sr and Nd isotope compositions with continental signatures, as do the North Makran granites with similar ages (Figure 12b). The few Sanandaj-Sirjan Zone intrusions geochemically comparable to the North Makran diorite-trondhjemite-plagiogranite sequence are also Late Jurassic (165–145 Ma) [*Omrani et al.*, 2008; *Shahbazi et al.*, 2010; *Azizi et al.*, 2011]. Like in Makran, their isotopic signatures ($^{87}Sr/^{86}Sr_{(i)}$ ~0.7022–0.7069 and $\varepsilon_{Nd(i)}$~2.1–4.9) suggest an increased mantle component with respect to the older granites (Figure 12b). These age and compositional similarities support the postulate of Sanandaj-Sirjan Zone continental lithosphere continuing into the Dur Kan Complex of North Makran before and during Jurassic times.

6.3.2. Were the Sanandaj-Sirjan Zone and Central Iran Connected up to the Jurassic?

The tectonic evolution of Iran is characterized by the opening and closure of the Paleotethys and Neotethys Oceans [*Alavi*, 1994]. There are two suggestions on the position of the Neotethys suture zone: (1) to the north of the Sanandaj-Sirjan Zone, which would then be part of the Arabian passive margin [e.g., *Falcon*, 1969; *Alavi*, 1980, 1994] and (2) to the southeast of the Sanandaj-Sirjan Zone, separating it from Arabia along the Zagros suture zone [*Berberian and King*, 1981; *Dercourt et al.*, 1986; *Şengör and Hsü*, 1984; *Ghasemi and Talbot*, 2006].

The Sanandaj-Sirjan Zone was part of Gondwana during most of the Paleozoic [*Stöcklin*, 1968; *Berberian and King*, 1981; *Alavi*, 1994; *Hassanzadeh et al.*, 2008; *Stampfli and Borel*, 2002; *Wendt et al.*, 2005]. Permian breakup and subsequent opening of the Neotethys Ocean separated the Sanandaj-Sirjan Zone and Central Iran from Arabia [*Şengör*, 1979, 1990; *Dercourt et al.*, 1986; *Ricou*, 1994; *Stampfli and Borel*, 2002;

Mohajjel et al., 2003; *Alavi*, 2004; *Agard et al.*, 2005; *Hassanzadeh et al.*, 2008; *Alirezaei and Hassanzadeh*, 2012]. This is manifested in the Eurasian affinity of post-Permian sediments in both the Sanandaj-Sirjan Zone and Central Iran [*Stöcklin*, 1968; *Berberian and King*, 1981]. Dominating platform and shallow water conditions in the Sanandaj-Sirjan Zone changed only in Upper Cretaceous [*Alavi and Mahdavi*, 1994], when flysch and turbidites discriminate it from the continental to shallow marine environment of Central Iran [*Mohajjel*, 1997], confirming that the two domains were part of the same tectonic unit. This is also consistent with the Dur Kan Complex stratigraphy, which represented a continental shelf during Carboniferous, Permian, and Jurassic and a carbonate fore-arc zone in Late Cretaceous(?) [*McCall et al.*, 1985; *McCall*, 2002].

There is no evidence for the presence of an oceanic basin (that would be witnesses by ophiolites today) between the Sanandaj-Sirjan Zone and Central Iran until the Jurassic. We conclude that they separated as one block from Gondwana during the Late Permian breakup of Pangea and drifted away during the Tethys opening behind. They split in the Jurassic, when an oceanic seaway or gulf (like the present-day Gulf of California) opened and formed the Nain-Dehshir-Baft ophiolites (Inner Zagros Ophiolites; Figure 1).

6.3.3. North Makran Ophiolites: Back-Arc or Marginal Basin?

There is a general consensus that the Makran subduction initiated in the Late Cretaceous [*Berberian and King*, 1981; *Desmons and Beccaluva*, 1983; *Babaie et al.*, 2001]. Jurassic subduction below the Sanandaj-Sirjan Zone was inferred from granitoids attributed to the volcanic arc [e.g., *Berberian and King*, 1981; *Mohajjel et al.*, 2003; *Sepahi and Athari*, 2006; *Ahmadi-Khalaji et al.*, 2007; *Mazhari et al.*, 2009; *Shahbazi et al.*, 2010; *Ahadnejad et al.*, 2011; *Esna-Ashari et al.*, 2012]. Concluding on subduction activity based only on geochemistry is fragile since calc-alkaline features suggest a mixed (mantle continent) source but not explicitly subduction [e.g., *Shand*, 1943; *Zen*, 1988; *Barbarin*, 1999]. Granitic melts may form through a wide range of processes from different sources, but for those originating from crustal anatexis, their final composition is mainly controlled by the composition of their protolith [e.g., *Beard et al.*, 2005; *Clemens et al.*, 2010; *Clemens and Stevens*, 2012]. The chemical characteristics of the Sanandaj-Sirjan and North Makran granites are marked by the contribution of the preexisting crust. Whether the basement has melted via heat advection of mantle-wedge magma in a subduction zone or lithospheric thinning during the opening of a basin can hardly be distinguished. Therefore, ascribing the Sanandaj-Sirjan granitoids to an Andean-type, Jurassic active margin is not a robust interpretation.

Our new data indicate that the North Makran Ophiolites are located in the same geotectonic position as the Inner Zagros Ophiolites (Nain-Dehshir-Baft complexes) between the Sanandaj-Sirjan Zone and Central Iran. The Inner Zagros Ophiolites is composed of mainly ultramafic rocks without an extensive isotropic gabbro sequence. Ultramafic rocks and locally overlying pillow lavas are intruded by several gabbro and diabase dikes [e.g., *Arvin and Robinson*, 1994; *Ghazi et al.*, 2012]. The geochemical signatures of the igneous rocks range from within plate to mid-ocean ridge to suprasubduction affinity [e.g., *Arvin and Robinson*, 1994; *Moghadam et al.*, 2009; *Ghazi et al.*, 2012]. Since the Nain-Dehshir-Baft complexes are tectonically disrupted, correlating chemical signal with age is not straightforward; however, available stratigraphy and radiometric dating suggest a Late Cretaceous age of the ophiolite [e.g., *Hassanipak and Ghazi*, 2000; *Moghadam et al.*, 2009].

The North Makran Ophiolites were also interpreted as remnants of the Tethys Ocean [*Şengör*, 1990; *Ricou*, 1994; *McCall*, 1997] but represent a "complete," mostly undisturbed sequence including extensive isotropic gabbro intrusions, diabase, and lavas with at least Barremian age [*Dolati*, 2010]. There is no obvious subduction signal in igneous rocks of the North Makran Ophiolites before Late Cretaceous lavas, which unconformably cover the older ophiolite [*Hunziker*, 2014]. The Inner Zagros Ophiolites, interpreted as a narrow back-arc basin of the hypothetical Sanandaj-Sirjan arc [*Moghadam et al.*, 2009], are thus comparable to the North Makran Ophiolites during their Late Cretaceous evolution. However, since there are no Early Cretaceous or older lavas reported in the Inner Zagros Ophiolite, their geochemical affinity cannot be justified. The earlier spreading state and larger volumes of isotropic gabbros during oceanic crust production in the Makran area could be related to the counterclockwise rotation of Central Iran during Jurassic [*Soffel et al.*, 1996]. If the Jurassic granitoids are extension related, as we propose, the Late Cretaceous units of Inner Zagros and North Makran Ophiolites represent a Jurassic-Early Cretaceous marginal basin transformed into the fore-arc region of the Urumieh Dokhtar arc in Late Cretaceous.

7. Conclusions

The North Makran granitoids are part of the continental Dur Kan Complex and show a multistage magmatic evolution with three magma sources operating at different times but recording extension:

1. Granites emplaced between 175–170 Ma into a carbonate shelf platform represent rifting-related magmatism from a continentally affected source into the Iranian margin of the Tethys Ocean.
2. The Middle to Upper Jurassic diorite-trondhjemite-plagiogranite (165–153 Ma) magmatic suite formed through low-pressure fractional crystallization of a mantle-derived parental melt that has been contaminated by continental crust, likely the preexisting Jurassic granites.
3. Diabase and lava intruded and covered exhumed and eroded granitoids in Early Cretaceous (~145 Ma) times. These mantle-derived alkaline magmas represent the spreading stage of the embryonic marginal basin that hosted the North Makran Ophiolites.

The North Makran granitoids are coeval with compositionally similar granitoids of the Sanandaj-Sirjan Zone; they are likely related to the same tectonic regime. We suggest extension-related magmatic activity along the Central Iranian continental margin in Late Jurassic and Early Cretaceous rather than the subduction-dominated magmatism proposed by previous studies.

Acknowledgments
Supplementary data can be obtained from the author upon request. This work was supported by the ETH research grant ETH-04 08–3. Pierre Bouilhol was partly supported by the ERC grant StG 279828. We are grateful for the logistical support of the Geological Survey of Iran, to Olivier Bruguier in Montpellier for his support with trace element solution analyses, and to Sergey Sergeev from the Center of Isotopic Research in St. Petersburg for SHRIMP analyses. We thank the two anonymous reviewers for their valuable comments which improved the manuscript.

References

Agard, P., J. Omrani, L. Jolivet, and F. Mouthereau (2005), Convergence history across Zagros (Iran): Constraints from collisional and earlier deformation, *Int. J. Earth Sci.*, *94*, 401–419.
Aghazadeh, M., A. Castro, N. R. Omran, M. H. Emami, H. Moinvaziri, and Z. B. (2010), The gabbro (shoshonitic)-monzonite-granodiorite association of Khankandi pluton, Alborz Mountains, NW Iran, *J. Asian Earth Sci.*, *38*, 199–219.
Ahadnejad, V., M. V. Valizadeh, R. Deevsalar, and M. Rezaei-Kahkhaei (2011), Age and geotectonic position of the Malayer granitoids: Implication for plutonism in the Sanandaj-Sirjan Zone, western Iran, *Neues Jahrbuch für Geologie und Palaontologie-Abhandlungen*, *261*, 61–75.
Ahmadi-Khalaji, A., D. Esmaeily, M. V. Valizadeh, and H. Rahimpour-Bonab (2007), Petrology and geochemistry of the granitoid complex of Boroujerd, Sanandaj-Sirjan Zone, western Iran, *J. Asian Earth Sci.*, *29*, 859–877.
Alavi, M. (1980), Tectonostratigraphic evolution of the Zagrosides of Iran, *Geology*, *8*(3), 144–149.
Alavi, M. (1994), Tectonics of the Zagros Orogenic Belt of Iran: New data and interpretations, *Tectonophysics*, *229*, 211–238.
Alavi, M. (1996), Tectonostratigraphic synthesis and structural style of the Alborz mountain system in northern Iran, *J. Geodyn.*, *21*, 1–33.
Alavi, M. (2004), Regional stratigraphy of the Zagros fold-thrust belt of Iran and its proforeland evolution, *Am. J. Sci.*, *304*(1), 1–20.
Alavi, M., and M. A. Mahdavi (1994), Stratigraphy and structures of the Nahavand region in western Iran, and their implications for the Zagros tectonics, *Geol. Mag.*, *131*(01), 43–47.
Alirezaei, S., and J. Hassanzadeh (2012), Geochemistry and zircon geochronology of the Permian A-type Hasanrobat granite, Sanandaj-Sirjan belt: A new record of the Gondwana breakup in Iran, *Lithos*, *151*, 122–134.
Arshadi-Khamseh, S. (1982), Geologische und Petrographische Untersuchungen des Fanuj-Gebietes (Baluchestan/Makran/SE-Iran) unter besonderer Berücksichtigung des Ophiolith-Komplexes, in *Fakultät für Bergbau und Hüttenwesen*, Technische Hochschule Aachen, Aachen.
Arvin, M., and P. T. Robinson (1994), The petrogenesis and tectonic setting of lavas from the Baft ophiolitic mélange, southwest of Kerman, Iran, *Can. J. Earth Sci.*, *31*(5), 824–834.
Azizi, H., Y. Asahara, B. Mehrabi, and S. L. Chung (2011), Geochronological and geochemical constraints on the petrogenesis of high-K granite from the Suffi Abad area, Sanandaj-Sirjan Zone, NW Iran, *Chem. Erde*, *71*, 363–376.
Babaie, H. A., A. M. Ghazi, A. Babaei, T. E. La Tour, and A. A. Hassanipak (2001), Geochemistry of arc volcanic rocks of the Zagros Crush Zone, Neyriz, Iran, *J. Asian Earth Sci.*, *19*(1–2), 61–76.
Barbarin, B. (1999), A review of the relationships between granitoid types, their origins, and their geodynamic environments, *Lithos*, *46*(3), 605–626.
Bayer, R., J. Chery, M. Tatar, P. Vernant, M. Abbassi, F. Masson, E. Nilforoushan, E. Doerflinger, V. Regard, and O. Bellier (2006), Active deformation in Zagros-Makran transition zone inferred from GPS measurements, *Geophys. J. Int.*, *165*, 373–381.
Beard, J. S., P. C. Ragland, and M. L. Crawford (2005), Reactive bulk assimilation: A model for crust-mantle mixing in silicic magmas, *Geology*, *33*(8), 681, doi:10.1130/g21470.1.
Berberian, M., and G. C. P. King (1981), Towards a paleogeography and tectonic evolution of Iran, *Can. J. Earth Sci.*, *18*, 210–265.
Burg, J.-P., A. Dolati, D. Bernoulli, and J. Smit (2013), Structural style of the Makran tertiary accretionary complex in SE Iran, in *Frontiers in Earth Sciences*, edited by K. Al Hosani et al., pp. 239–259.
Carter, A., Y. Najman, A. Bahroudi, P. Bown, E. Garzanti, and R. D. Lawrence (2010), Locating earliest records of orogenesis in western Himalaya: Evidence from Paleogene sediments in the Iranian Makran region and Pakistan Katawaz basin, *Geology*, *38*(9), 807–810.
Chappell, B. W., and A. J. R. White (1974), Two contrasting granite types, *Pac. Geol.*, *8*, 173–174.
Clemens, J. D. (1998), Observations on the origins and ascent mechanisms of granitic magmas, *J. Geol. Soc.*, *155*(5), 843–851.
Clemens, J. D., and G. Stevens (2012), What controls chemical variation in granitic magmas?, *Lithos*, *134*, 317–329.
Clemens, J. D., P. A. Helps, and G. Stevens (2010), Chemical structure in granitic magmas: A signal from the source?, *Earth Environ. Sci. Trans. R. Soc. Edinburgh*, *100*(1–2), 159–172, doi:10.1017/s1755691009016053.
Coleman, R. G., S. DeBari, and Z. Peterman (1992), A-type granite and the Red Sea opening, *Tectonophysics*, *204*, 27–40.
Cox, K. G., J. D. Bell, and R. J. Pankhurst (1979), *The Interpretation of Igneous Rocks*, Allen and Unwin, London.
Dercourt, J., et al. (1986), Geological evolution of the Tethys Belt from the Atlantic to the Pamirs since the Lias, *Tectonophysics*, *123*, 241–315.
Desmons, J., and L. Beccaluva (1983), Mid-Ocean ridge and island-arc affinities in ophiolites from Iran: Paleographic implications, *Chem. Geol.*, *39*(1–2), 39–63.
Dilek, Y., P. Thy, B. Hacker, and S. Grundvig (1999), Structure and petrology of Tauride ophiolites and mafic dike intrusions (Turkey): Implications for the Neotethyan Ocean, *Geol. Soc. Am. Bull.*, *111*, 1192–1216.

Dolati, A. (2010), Stratigraphy, structural geology, and low-temperature thermochronology across the Makran accretionary wedge in Iran, PhD thesis, pp. 1–210, Dep. of Earth Sci., Swiss Inst. of Technol. (ETH), Zurich, Switzerland.
Dunham, A. C. (1965), The nature and origin of groundmass textures in felsites and granophyres from Rhum, Inverness-shire, *Geol. Mag.*, *102*, 8–23.
Eftekhar-Nezhad, J., S. Arshadi, M. A. Mahdavi, K. H. Morgan, G. J. H. McCall, and H. Huber (1979), Fannuj Quadrangle Map 1:250'000, in *Ministry of Mines and Metal*, Geol. Surv. of Iran, Tehran.
Esmaeily, D., A. Nelelec, M. V. Valizadeh, F. Moore, and J. Cotten (2005), Petrology of the Jurassic Shah-Kuh granite (eastern Iran), with reference to tin mineralization, *J. Asian Earth Sci.*, *25*(6), 961–980.
Esna-Ashari, A., M. Tiepolo, M. V. Valizadeh, J. Hassanzadeh, and A. A. Sepahi (2012), Geochemistry and zircon U-Pb geochronology of Aligoodarz granitoid complex, Sanandaj-Sirjan Zone, Iran, *J. Asian Earth Sci.*, *43*, 11–22.
Falcon, N. L. (1969), Problems of the relationship between surface structure and deep displacements illustrated by the Zagros Range, *Geol. Soc. London Spec. Publ.*, *3*(1), 9–21.
Farhoudi, G., and D. E. Karig (1977), Makran of Iran and Pakistan as an active arc system, *Geology*, *5*, 664–668.
Fazlnia, A., V. Schenk, F. Straaten, and M. Mirmohammadi (2009), Petrology, geochemistry, and geochronology of trondhjemites from the Qori Complex, Neyriz, Iran, *Lithos*, *112*(3–4), 413–433.
Ghasemi, A., and C. J. Talbot (2006), A new tectonic scenario for the Sanandaj-Sirjan Zone (Iran), *J. Asian Earth Sci.*, *26*, 683–693.
Ghazi, J. M., M. Moazzen, M. Rahgoshay, and H. S. Moghadam (2012), Geochemical characteristics of basaltic rocks from the Nain ophiolite (central Iran): Constraints on mantle wedge source evolution in an oceanic back arc basin and a geodynamical model, *Tectonophysics*, *574*, 92–104.
Haghipour, N., J.-P. Burg, F. Kober, G. Zeilinger, S. Ivy-Ochs, P. W. Kubik, and M. Faridi (2012), Rate of crustal shortening and non-Coulomb behavior of an active accretionary wedge: The folded fluvial terraces in Makran (SE, Iran), *Earth Planet. Sci. Lett.*, *355*, 187–198.
Harris, N. B. W., J. A. Pearce, and A. G. Tindle (1986), Geochemical characterisitcs of collision-zone magmatism, *Geol. Soc. London Spec. Publ.*, *19*, 67–81.
Hassanipak, A. A., and A. M. Ghazi (2000), Petrology, geochemistry, and tectonic setting of the Khoy ophiolite, northwest Iran: Implications for Tethyan tectonics, *J. Asian Earth Sci.*, *18*(1), 109–121.
Hassanzadeh, J., D. F. Stockli, B. K. Horton, G. J. Axen, L. D. Stockli, M. Grove, A. K. Schmitt, and J. D. Walker (2008), U-Pb zircon geochronology of late Neoproterozoic-Early Cambrian granitoids in Iran: Implications for paleogeography, magmatism, and exhumation history of Iranian basement, *Tectonophysics*, *451*, 71–96.
Hoskin, P. W. O., and U. Schaltegger (2003), The composition of zircon and igneous and metamorphic petrogenesis, in *Zircon*, Review in Mineralogy and Geochemistry, vol. 53, edited by J. M. Hanchar and P. W. O. Hoskin, pp. 27–62, Mineral. Soc. of Am., Washington, D. C.
Hunziker, D. (2014), Magmatic and metamorphic history of the North Makran ophiolites and blueschists (SE Iran): Influence of Fe^{3+}/Fe^{2+} ratios in blueschist facies minerals on geothermobarometric calculations, PhD thesis, pp. 1–364, Dep. of Earth Sci., Swiss Inst. of Technol. (ETH), Zurich, Switzerland.
International Chronostratigraphic Chart 2014/02 (2014), International Commission of Stratigraphy. [Available at http//www.stratigraphy.org/ICSchart/ChronostratChart2014-02.pdf.]
Irvine, T. N., and W. R. A. Baragar (1971), Guide to chemical classification of common volcanic rocks, *Can. J. Earth Sci.*, *8*, 523–548.
Jacobsen, S. B., and G. J. Wasserburg (1984), Sm-Nd isotopic evolution of chondrites and achondrites, II, *Earth Planet. Sci. Lett.*, *67*(2), 137–150.
Johannes, W., and F. Holtz (1991), Formation and ascent of granitic magmas, *Geol. Rundsch.*, *80*(2), 225–231.
Karimpour, M. H., C. R. Stern, L. Farmer, S. Saadat, and A. Malekezadeh (2011), Review of age, Rb-Sr geochemistry, and petrogenesis of Jurassic to Quaternary igneous rocks in Lut Block, eastern Iran, *GeoPersia*, *1*(1), 19–36.
Kelemen, P. B., K. Hanghoj, and A. R. Greene (2003), One view of the geochemistry of subduction-related magmatic arcs, with an emphasis on primitive andesite and lower crust, in *Treatise on Geochemistry*, edited by H. D. Holland and K. K. Turekian, pp. 1–70, Elsevier, Amsterdam.
Khalaji, A. A., D. Esmaeily, M. V. Valizadeh, and H. Rahimpour-Bonab (2007), Petrology and geochemistry of the granitoid complex of Boroujerd, Sanandaj-Sirjan Zone, western Iran, *J. Asian Earth Sci.*, *29*, 859–877.
Kretz, R. (1983), Symbols for rock-forming minerals, *Am. Mineral.*, *68*, 277–279.
Krogh, T. E. (1982), Improved accuracy of U-Pb zircon ages by the creation of more concordant systems using an air abrasion technique, *Geochimica Cosmochimica Acta*, *46*, 637–649.
Marrett, R., and R. W. Allmendinger (1990), Kinematic analysis of fault-slip data, *J. Struct. Geol.*, *12*, 973–986.
Mattinson, J. M. (2005), Zircon U-Pb chemical abrasion ("CA-TIMS") method: Combined annealing and multistep partial dissolution analysis for improved precision and accuracy of zircon ages, *Chem. Geol.*, *220*(1), 47–66.
Mazhari, S. A., F. Bea, S. Amini, J. Ghalamghash, J. F. Molina, P. Montero, J. H. Scarrow, and I. S. Williams (2009), The Eocene bimodal Piranshahr massif of the Sanandaj-Sirjan Zone, NW Iran: A marker of the end of the collision in the Zagros orogen, *J. Geol. Soc.*, *166*, 53–69.
McCall, G. J. H. (1997), The geotectonic history of the Makran and adjacent areas of southern Iran, *J. Asian Earth Sci.*, *15*, 517–531.
McCall, G. J. H. (2002), A summary of the geology of the Iranian Makran, *Tectonic Clim. Evol. Arabian Sea Region*, *195*, 147–204.
McCall, G. J. H., and R. G. W. Kidd (1982), The Makran, southeastern Iran: The anatomy of a convergent plate margin active from Cretaceous to present, in *Trench-Fore-Arc Geology: Sedimentation and Tectonics on Modern and Ancient Active Plate Margins, Conference*, edited by K. L. Jeremy, pp. 387–397, Geol. Soc. of London, U. K.
McCall, G. J. H., J. Eftekhar-Nezhad, M. Samimi-Namin, and S. Arshadi (1985), Explanatory text of the Fannuj quadrangle map 1:250,000, in *Ministry of Mines and Metals*, edited by G. J. H. McCall, Geol. Surv. of Iran, Tehran.
Moghadam, H. S., M. Rahgoshay, and A. Banitaba (2009), Geochemistry and petrogenesis of basaltic flows in the Nain-Dehshir ophiolites, *Iranian Soc. Cryst. Mineral.*, *16*, 603–612.
Mohajjel, M. (1997), Structure and tectonic evolution of Palaeozoic-Mesozoic rocks, Sanandaj-Sirjan Zone, western Iran, PhD thesis, Univ. of Wollongong, Australia.
Mohajjel, M., C. L. Fergusson, and M. R. Sahandi (2003), Cretaceous-tertiary convergence and continental collision, Sanandaj-Sirjan Zone, western Iran, *J. Asian Earth Sci.*, *21*, 397–412.
Omrani, J., P. Agard, H. Whitechurch, M. Benoit, G. Prouteau, and L. Jolivet (2008), Arc-magmatism and subduction history beneath the Zagros Mountains, Iran: A new report of adakites and geodynamic consequences, *Lithos*, *106*, 380–398.
Pearce, J. A., and D. W. Peate (1995), Tectonic implications of the composition of volcanic arc magmas, *Annu. Rev. Earth Planet. Sci.*, *23*, 251–285.
Pearce, J. A., N. B. W. Harris, and A. G. Tindle (1984), Trace-element discrimination diagrams for the tectonic interpretation of granitic rocks, *J. Petrol.*, *25*, 956–983.

Pidgeon, R. T. (1992), Recrystallization of oscillatory zoned zircon: Some geochronological and petrological implications, *Contrib. Mineral. Petrol.*, *110*, 463–472.
Pitcher, W. S. (1979), The nature, ascent, and emplacement of granitic magmas, *J. Geol. Soc.*, *136*(6), 627–662.
Puga, E., C. M. Fanning, J. M. Nieto, and A. Díaz de Federico (2005), Recrystallization textures in zircon generated by ocean floor metamorphism and eclogite-facies metamorphism: A cathodoluminescence and U-Pb SHRIMP study, with constraints from REE elements, *Can. Mineral.*, *43*, 183–202.
Ricou, L. E. (1994), Tethys reconstructed - plates, continental fragments and their boundaries since 260 Ma from central-America to outheastern Asia, *Geodinamica Acta*, *7*, 169–218.
Ruh, J. B., T. Gerya, and J. P. Burg (2013), High-resolution 3-D numerical modeling of thrust wedges: Influence of décollement strength on transfer zones, *Geochem. Geophys. Geosyst.*, *14*, 1131–1155, doi:10.1002/ggge.20085.
Savostin, L. A., J. C. Sibuet, L. P. Zonenshain, X. Le Pichon, and M. J. Roulet (1986), Kinematic evolution of the Tethys belt from the Atlantic Ocean to the Pamirs since the Triassic, *Tectonophysics*, *123*(1), 1–35.
Scotese, C. (2004), A continental drift flipbook, *J. Geol.*, *112*, 729–741.
Şengör, A. M. C. (1979), The North Anatolian transform fault: Its age, offset, and tectonic significance, *J. Geol. Soc.*, *136*(3), 269–282.
Şengör, A. M. C. (1990), A new model for the Late Paleozoic Mesozoic tectonic evolution of Iran and implications for Oman, *Geol. Tectonics Oman Reg.*, *49*, 797–831.
Şengör, A. M. C., and K. J. Hsü (1984), The Cimmerides of eastern Asia: History of the eastern end of Paleotethys, *Mem. Soc. Geol. France*, *147*, 139–167.
Sepahi, A. A., and S. F. Athari (2006), Petrology of major granitic plutons of the northwestern part of the Sanandaj-Sirjan Metamorphic Belt, Zagros Orogen, Iran: With emphasis on A-type granitoids from the SE Saqqez area, *Neues Jahrbuch Fur Mineralogie-Abhandlungen*, *183*, 93–106.
Shahabpour, J. (2010), Tectonic implications of the geochemical data from the Makran igneous rocks in Iran, *Island Arc*, *19*, 676–689.
Shahbazi, H., W. Siebel, M. Pourmoafee, M. Ghorbani, A. A. Sepahi, C. K. Shang, and M. V. Abedini (2010), Geochemistry and U-Pb zircon geochronology of the Alvand plutonic complex in Sanandaj-Sirjan Zone (Iran): New evidence for Jurassic magmatism, *J. Asian Earth Sci.*, *39*, 668–683.
Shand, S. J. (1943), *Eruptive Rocks: Their Genesis, Composition, Classification, and Their Relations to Ore Deposits*, 444 pp., Wiley, New York.
Soffel, H. C., S. Schmidt, M. Davoudzadeh, and C. Rolf (1996), New palaeomagnetic data from central Iran and a Triassic palaeoreconstruction, *Geol. Rundsch.*, *85*(2), 293–302.
Stampfli, G. M., and G. D. Borel (2002), A plate tectonic model for the Paleozoic and Mesozoic constrained by dynamic plate boundaries and restored synthetic oceanic isochrons, *Earth Planet. Sci. Lett.*, *196*, 17–33.
Stöcklin, J. (1968), Structural history and tectonics of Iran: A review, *Am. Assoc. Pet. Geol. Bull.*, *52*, 1229–1258.
Streckeisen, A. L. (1976), To each plutonic rock its proper name, *Earth Sci. Rev.*, *12*, 1–33.
Sun, S. S., and W. F. McDonough (1989), Chemical and isotopic systematics of ocean basalts: Implications for mantle composition and processes, in *Magmatism in the Ocean Basins*, edited by A. D. Saunder and M. J. Norry, *Geol. Soc. London Spec. Publ., 42*, 313–345.
Vavra, G. (1990), On the kinematics of zircon growth and its petrogenetic significance: A cathodoluminescence study, *Contrib. Mineral. Petrol.*, *106*, 90–99.
Vigny, C., P. Huchon, J. C. Ruegg, K. Khanbari, and L. M. Asfaw (2006), Confirmation of Arabia plate slow motion by new GPS data in Yemen, *J. Geophys. Res.*, *111*, B02402, doi:10.1029/2004JB003229.
Wendt, J., B. Kaufmann, Z. Belka, N. Farsan, and A. K. Bavandpur (2005), Devonian/Lower Carbonifeous stratigraphy, facies patterns, and palaeogeography of Iran: Part II. Northern and central Iran, *Acta Geologica Polonica*, *55*(1), 31–97.
Westphal, M., M. L. Bazhenov, J. P. Lauer, D. M. Pechersky, and J. C. Sibuet (1986), Paleomagnetic implications on the evolution of the Tethys belt from the Atlantic Ocean to the Pamirs since the Triassic, *Tectonophysics*, *123*(1), 37–82.
Whitney, D. L., and B. W. Evans (2010), Abbreviations for names of rock-forming minerals, *Am. Mineral.*, *95*, 185–187.
Zen, E.-A. (1988), Phase relations of peraluminous granitic rocks and their petrogenetic implications, *Annu. Rev. Earth Planet. Sci.*, *16*, 21–51.